Journal of Structural Geology 116 (2018) 189–206

Contents lists available at ScienceDirect

Journal of Structural Geology

journal homepage: www.elsevier.com/locate/jsg

Along-strike fault core thickness variations of a fault in poorly lithified sediments, Miri (Malaysia)

Silvia Sosio De Rosa[a,*], Zoe K. Shipton[a], Rebecca J. Lunn[a], Yannick Kremer[a], Titus Murray[b]

[a] Department of Civil and Environmental Engineering, University of Strathclyde, G1 1XJ, 75 Montrose St., Glasgow, UK
[b] FaultSeal Pty Ltd, Sydney, Australia

ARTICLE INFO

Keywords:
Fault core
Along-strike thickness
Variogram
Clay smear

ABSTRACT

The degree to which a fault will impede fluid flow is only as great as its most permeable point. Processes that determine areas of the fault surface containing transmissible fault rocks must be utilized to produce reliable predictions of cross-fault fluid flow. We use a study site in Miri, Malaysia, to investigate in detail the fault-core thickness variations along-strike and down dip, and to quantify the risk of discontinuities in the clay-rich fault core.

Four fault-core types have been identified: foliated clay-rich fault core, chaotic clay-rich fault core, anastomosing sandy shear zones and sandy breccia. We performed a geostatistical analysis, showing a correlation over 3 m scale, suggesting the presence of 'patches' of thin and thick fault core generally less than 3 m in length in profile.

We interpret this geometry as superimposition of two or more different deformation processes at a smaller and a larger scale. We speculate about the processes that could produce the observed distribution of thickness and composition, and in particular, processes that could have disrupted the through-going clay-rich core.

1. Introduction

Faults play a key role in controlling fluid flow in the shallow crust (Caine and Minor, 2009; Faulkner et al., 2010). Predicting bulk fault-zone petrophysical properties at depth is a key part of de-risking geological applications such as extraction of hydrocarbons, geothermal heat, storage of CO_2, or radioactive waste (Aydin, 2000; Douglas et al., 2000; Shipton et al., 2004). To predict whether faults act as barriers, baffles or conduits, structural geologists have attempted to develop relationships between key parameters of fault architecture, for example, using throw to predict mean fault thickness (Childs et al., 2007; Shipton et al., 2006), using host rock type and throw to predict fault-rock type (Faerseth, 2006), and then using these relationships to predict petrophysical properties. However, data from oil and gas production show that these estimates are not always reliable (Bretan et al., 2003). Field data show that this lack of reliability could be a consequence of significant along-strike variability within the fault plane due to fault-scale processes that are not only related to throw (Caine and Minor, 2009; Kremer et al., 2018).

It is the size and location of relatively high-permeability fault rocks, more than the mean low-permeability fault core thickness, that has the strongest influence on the hydraulic behaviour of a fault (Heynekamp et al., 1999; Lunn et al., 2008; Caine and Minor, 2009). Field studies of fault architecture generally focus on down-dip sections to determine the relationship between fault properties and stratigraphy. However, the along-strike dimension has to be investigated to constrain the probability of high-permeability areas in a low-permeability fault core. Significant lengths of along-strike sections are less commonly exposed, and so a dearth of published observations exists about along-strike variability.

Few studies of along-strike fault core composition have been published in siliciclastic, poorly consolidated sediments. Along-strike clay smear continuity was investigated by Lehner and Pilaar (1997) in a fault of 70 m throw cutting a sand-shale deltaic sequence in the Frechen mines (Germany). Doughty (2003) studied a 40–60 m throw growth fault in conglomerate and sand, silt and mud fluvial and lacustrine sediments. Van der Zee and Urai (2005) studies faults of up to a few m slip in the deltaic sediments of the Miri Formation. Kettermann et al. (2016) studied faults of 50–120 cm throw in deltaic sand-clay sequences. Lehner and Pilaar (1997) observe along-strike clay continuity over considerable distances, up to 400 m. In contrast, Doughty (2003), Van der Zee and Urai (2005) and Kettermann et al. (2016) found that

* Corresponding author.
E-mail addresses: silvia.sosio-de-rosa@strath.ac.uk (S. Sosio De Rosa), zoe.shipton@strath.ac.uk (Z.K. Shipton), rebecca.lunn@strath.ac.uk (R.J. Lunn), yannick.kremer@strath.ac.uk (Y. Kremer), titus@faultseal.com (T. Murray).

https://doi.org/10.1016/j.jsg.2018.08.012
Received 27 March 2018; Received in revised form 23 August 2018; Accepted 23 August 2018
Available online 25 August 2018

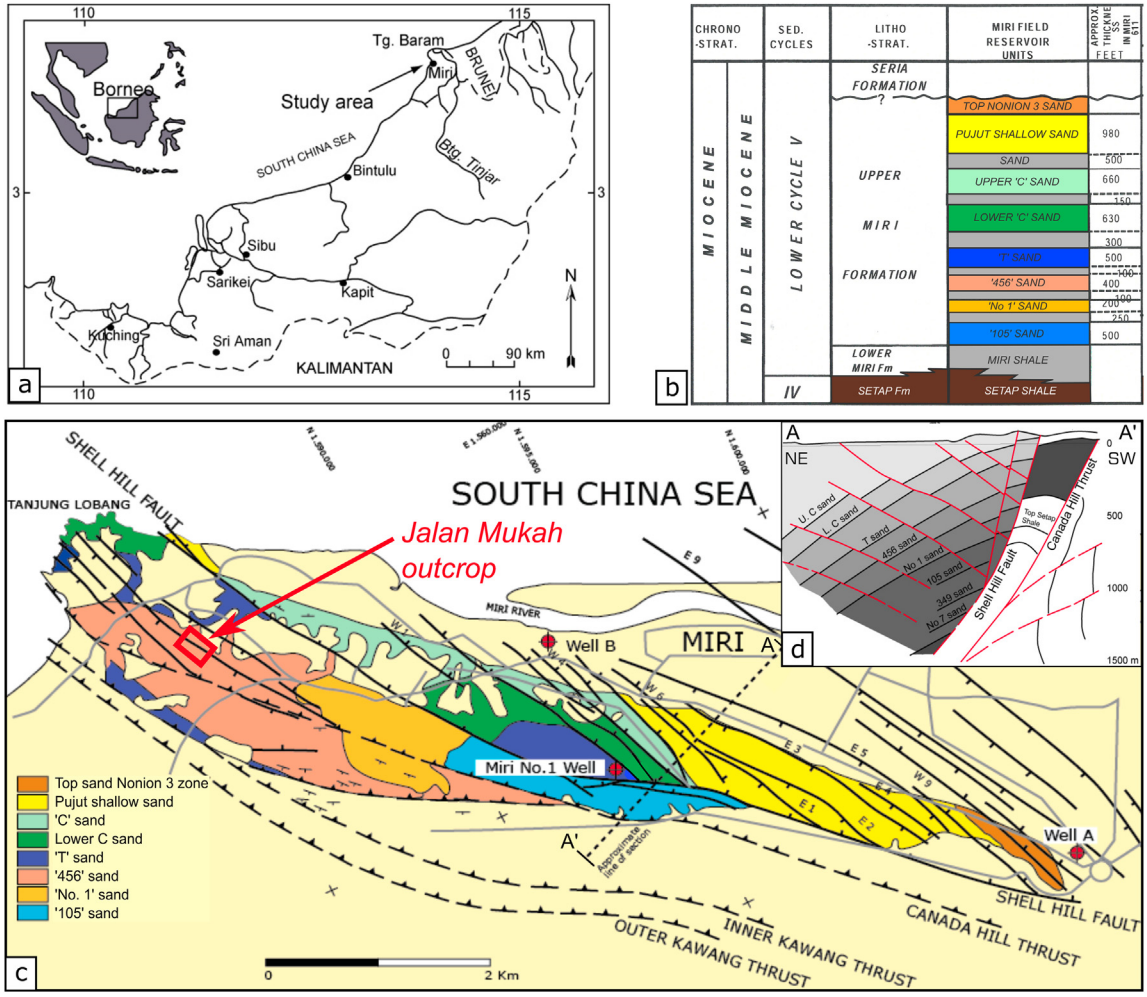

Fig. 1. a) Location of the study area in NW Borneo. b) Upper Miri Formation stratigraphy (modified after Wannier et al., 2011). c) Geological map and location of the Jalan Mukah outcrop (after Wannier et al., 2011). d) SW-NE cross section of the Miri anticline (Van der Zee and Urai, 2005).

clay smears were not continuous along-strike at the 100-m, m and dm scale respectively. The factors governing these differing observations are not well understood.

We present data from a site in soft sediments that offers extensive along-strike fault exposures and three sub-vertical cuts, giving an excellent 3D view of within-plane fault variability. We use spatial statistics (e.g. variogram analysis, Matheron, 1971) to characterize deformation processes, and provide key information for robust representation of these phenomena in numerical simulations. In agreement with Caine and Minor (2009) and Kremer et al. (2018), the variations that we observe cannot be related in a simple way to fault throw. Instead we demonstrate that a number of processes for incorporating the host rock materials into the fault zone are responsible for generating highly heterogeneous fault rocks along-strike.

2. Geological setting

The study area is located in Northwest Borneo, just outside the town of Miri (Fig. 1a). The stratigraphic sequence of the Jalan Mukah outcrop is part of the 456 Sand of the Upper Miri Formation, Middle Miocene. The West Baram Delta is composed of up to 10 km of Middle Miocene to recent deltaic sequences (Tan et al., 1999). Marine shale intervals are separated by thicker coastal-fluviomarine sands, which constitute the producing reservoirs of the oil Miri field (Fig. 1b; Tan et al., 1999). Northwest Borneo is characterized by young gravity-related deformation: seaward (NW) and landward (SE) dipping growth faults, mobile shales, and toe thrusts (Morley et al., 2003). The Late Miocene gravity-driven extension is expressed in the Miri Hill structure as a set of listric faults, the most important of which is the Shell Hill fault (offset 750 m; Hutchinson, 2005), and its associated antithetic normal faults. The extension was followed by NW-SE Pliocene compression, which resulted in the reactivation of the Canada Hill Thrust and development of the Miri anticline (Fig. 1c and d), causing uplift of the landward side of the delta (Tan et al., 1999; Morley et al., 2003; Hutchinson, 2005; Wannier et al., 2011). A strike-slip component of deformation associated with compressional structures has been described by Sandal (1996) for high-angle faults in the Northwest Borneo margin.

The Jalan Mukah outcrop is located on the southern apex of the Miri anticline structure (Fig. 1c). Two sections of the outcrop were previously studied by Noorsalehi-Garakani (2015) for lateral clay injection mechanism, and by Kessler and Jong (2017) for clay smearing. This study is the first to describe all of the exposed sections and to analyse the along-strike fault-core thickness data with variograms. Other parts of this fault system have been previously studied (Burhannudinnur and Morley, 1997; Tan et al., 1999; Van der Zee et al., 2003; Van der Zee and Urai, 2005; Wannier et al., 2011). Van der Zee and Urai (2005) describe the initial evolution of normal faults in layered sand-clay sequences in the same formation, at the Airport road outcrop, about 300 m from the Jalan Mukah outcrop. The Jalan Mukah outcrop offers unprecedented along-strike exposure due to the clearing of an area of land of 1 km^2 for the installation of a large water tank, and three sub-vertical faces cut by bulldozer showing the faults in dip section

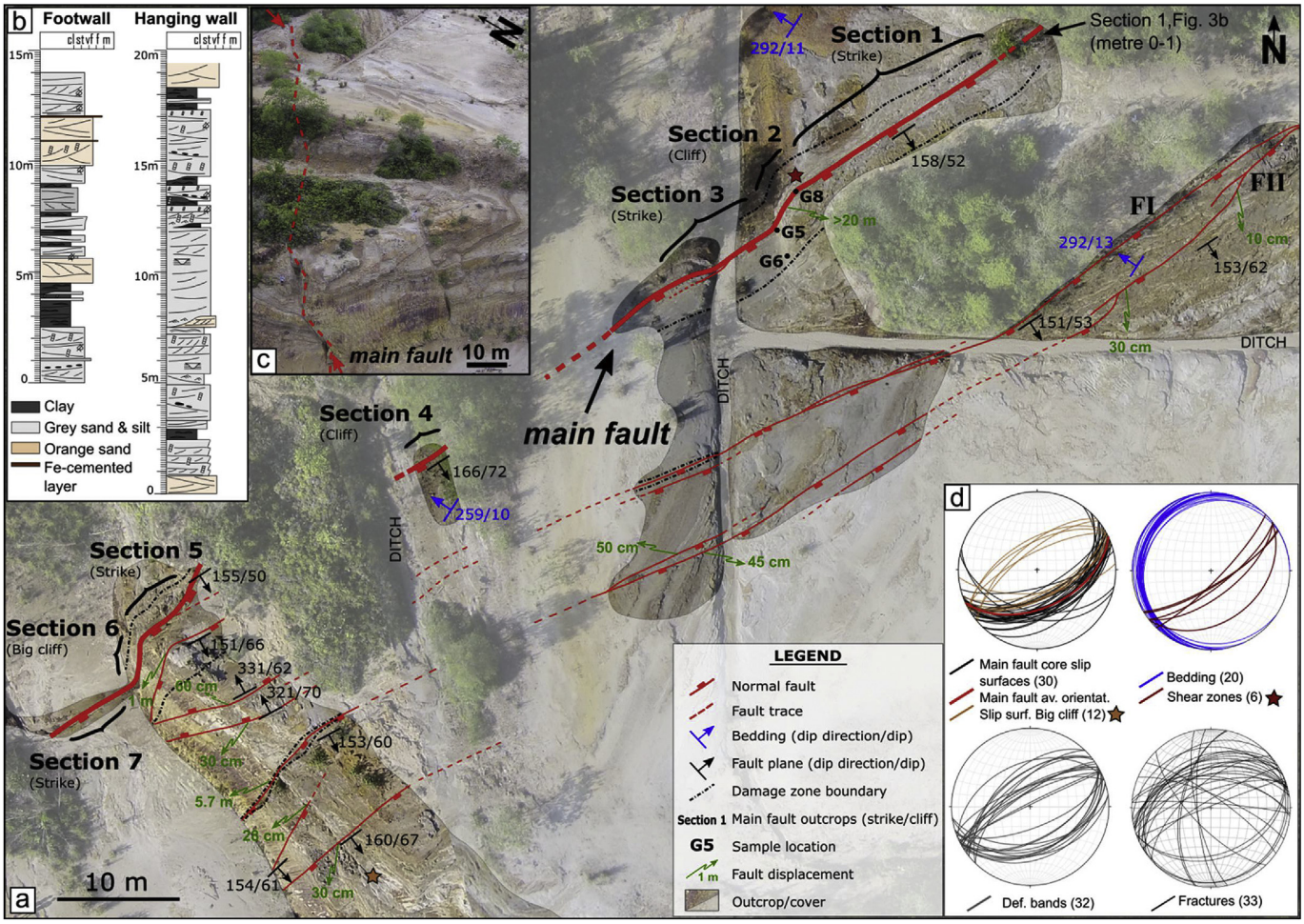

Fig. 2. Structural map of the Jalan Mukah outcrop showing the main fault (thick fault trace) and the secondary faults FI and FII (a). b) Footwall and hangingwall stratigraphy. c) Aerial picture of outcrop (45° view from SW). d) Stereographic projections of fault core slip surfaces, bedding and shear zones, deformation bands, fractures (lower hemisphere, equal area projections).

(Fig. 2a).

At the Jalan Mukah outcrop, the 456 Sand is dominated by grey fine to medium sand beds, with minor orange sands and interbedded clay-rich beds 0.2–2 m thick (Fig. 2b). The thickness and lateral distribution of sand and clay beds varies. Fossil Ophiomorpha burrows 1–10 cm long are common both in sand and clay beds. No calcite was observed either as sand grains, as cement, or as fracture fill. The maximum burial depth at the time of faulting was less than 1000 m, as indicated by clay porosity and vitrinite reflectance (Schmitz et al., 2003).

3. Methodology

A structural map of the whole outcrop (scale 1:500, resolution 50 cm), was compiled using high resolution photographs taken with a drone (Fig. 2a). A map of the fault with the largest displacement, referred to as 'main fault', was made at the 1:50 scale in the field. This map includes all structures with a length over 10 cm. The main fault was logged with a measuring tape along its entire length at every 0.5 m. The fault outcrop is exposed in both the planar and vertical dimensions along strike, and therefore the outcrops are divided into seven sections, which either expose the fault along strike or in a sub-vertical cliff. The logging of the main fault is complimented by measurements of the fault core (*sensu* Caine et al., 1996), and thickness and photographs of the fault zone, taken every 0.5 m. Vertical and selected parts of the along-strike exposures were mapped with a regular square grid of 0.5 × 0.5 m, placed with string and nails (Figs. 3–8). Photographs of grid squares were used as a base for tracing structural elements and data on site. Deformation band (DB), deformation-band cluster and fracture intensity within the fault damage zone were measured every 0.5 m along seven transects perpendicular to the main fault. Oriented samples were collected for microstructural analysis from the host rocks and the fault zone with hammer and knife (locations on Fig. 2). Extreme care was used to avoid the fragile rock crumbling into pieces. Footwall and hangingwall stratigraphy were logged.

4. Jalan Mukah outcrop

4.1. Main fault

The main fault of the Jalan Mukah outcrop trends ENE-WSW and dips SE between 40 and 62° (Fig. 2a and c). The main fault is traced for a length of about 100 m of which 55 m are exposed, and is associated with a conjugate set of normal faults with the same trend that dip 45–70° to the NNW and SSE (Fig. 2a and d). The main fault displaces the entire exposed stratigraphy, therefore it is not possible to correlate between the footwall and the hangingwall sequences which both belong to the 456 Sand unit. The main fault offset is constrained to a minimum offset by the thickness of the hangingwall stratigraphy (20 m), and the thickness of the 456 Sand (122 m). Kessler and Jong (2017) suggest a fault throw of 40–50 m based on litho-stratigraphic correlation, while Noorsalehi-Garakani (2015) suggests a throw of 20 m. The bedding consistently dips 10-15° west (Fig. 2d). Two synthetic faults in the

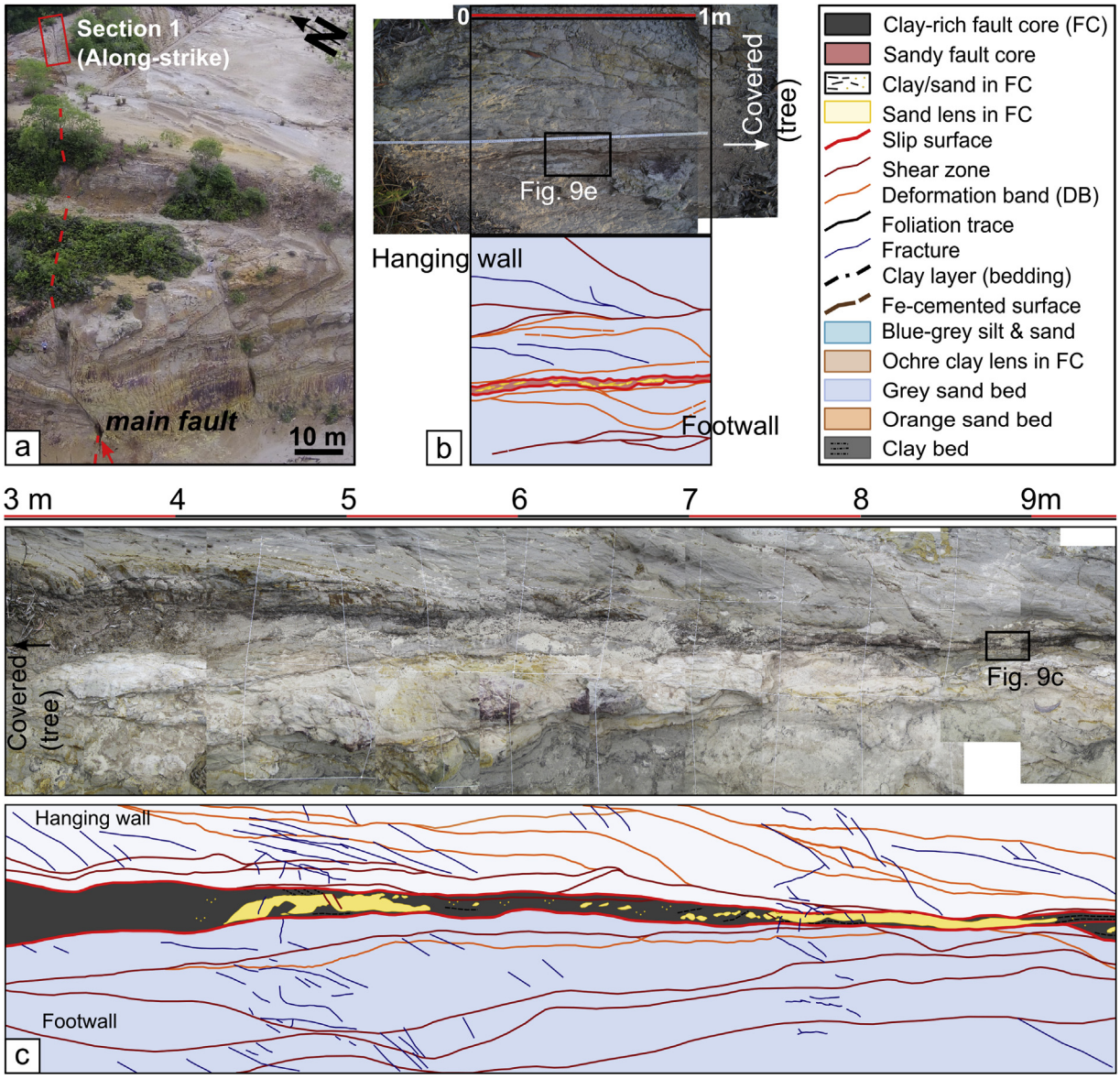

Fig. 3. Along-strike exposure of the main fault at section 1 (first half of the 25 m-long exposure). a) Location of section 1 along the main fault trace. b) Main fault with sand and silt-dominated fault core: picture (top) and map (bottom). Location of Fig. 9e is indicated and legend on the right. c) Continuation of the same outcrop where fault core is clay-rich and location of Fig. 9c is indicated.

hangingwall have throws of 5.7–8 m each (faults FI and FII, Fig. 2a), while all other conjugate faults have offsets smaller than 1 m. The lack of slickenlines on the slip surfaces prevents the determination of the sense of shear, however the inferred conjugate fault geometry indicates extensional normal dip-slip faults. A dextral component of shear is suggested by σ–shaped sand lenses in the clay-rich matrix of the fault core within sections 1 and 5.

The damage zone of the main fault at Jalan Mukah contains deformation bands, shear zones and gentle folds of clay and sand beds towards the fault core. Shear zones and deformation bands are defined as tabular structural discontinuities having a continuous change in strength or stiffness across a relatively narrow zone (Schultz and Fossen, 2008). In this field area, we distinguish shear zones from deformation bands because shear zones contain clay as well as sand, and generally have a larger offset for their width than deformation bands. Deformation bands are dominant in clean sand, while shear zones dominate where the host rock sands are more clay-rich. Deformation bands occur in conjugate sets trending NE-SW, dip towards SE and NW (34°–88°), matching the conjugate fault orientations, and have offsets of a few mm up to 5 cm. Shear zones have a similar orientation to the main fault, trending NE-SW and dipping 36 to 80° SE (Fig. 2d). Shear zones have offsets greater than few cm, with a maximum of 54 cm in the footwall and more than 1 m in the hangingwall.

The total damage-zone thickness varies from 1.5 to 7 m (core is bounded by black dashed lines on Fig. 2a). The damage zone limit is defined as the area where the deformation band density drops to a background level (4–6 DBs per 0.5 m). This width for a damage zone for the likely throw on the main fault is small, but is within the data population presented by Shipton et al. (2006) and Childs et al. (2007). The hangingwall damage zone is generally wider (3.5–7 m) than the footwall damage zone (1.5–2.5 m). Post-faulting fractures overprint the structures of interest with a variety of orientations (Fig. 2d) and vein-fill is absent. Sections 1–6 were used to characterize the fault core of the main fault in detail.

4.1.1. Section 1– Along strike

Starting from the NE end of the main fault, the first exposure is the along-strike, 25 m-long section 1 (Figs. 2 and 3a). The host rock on both

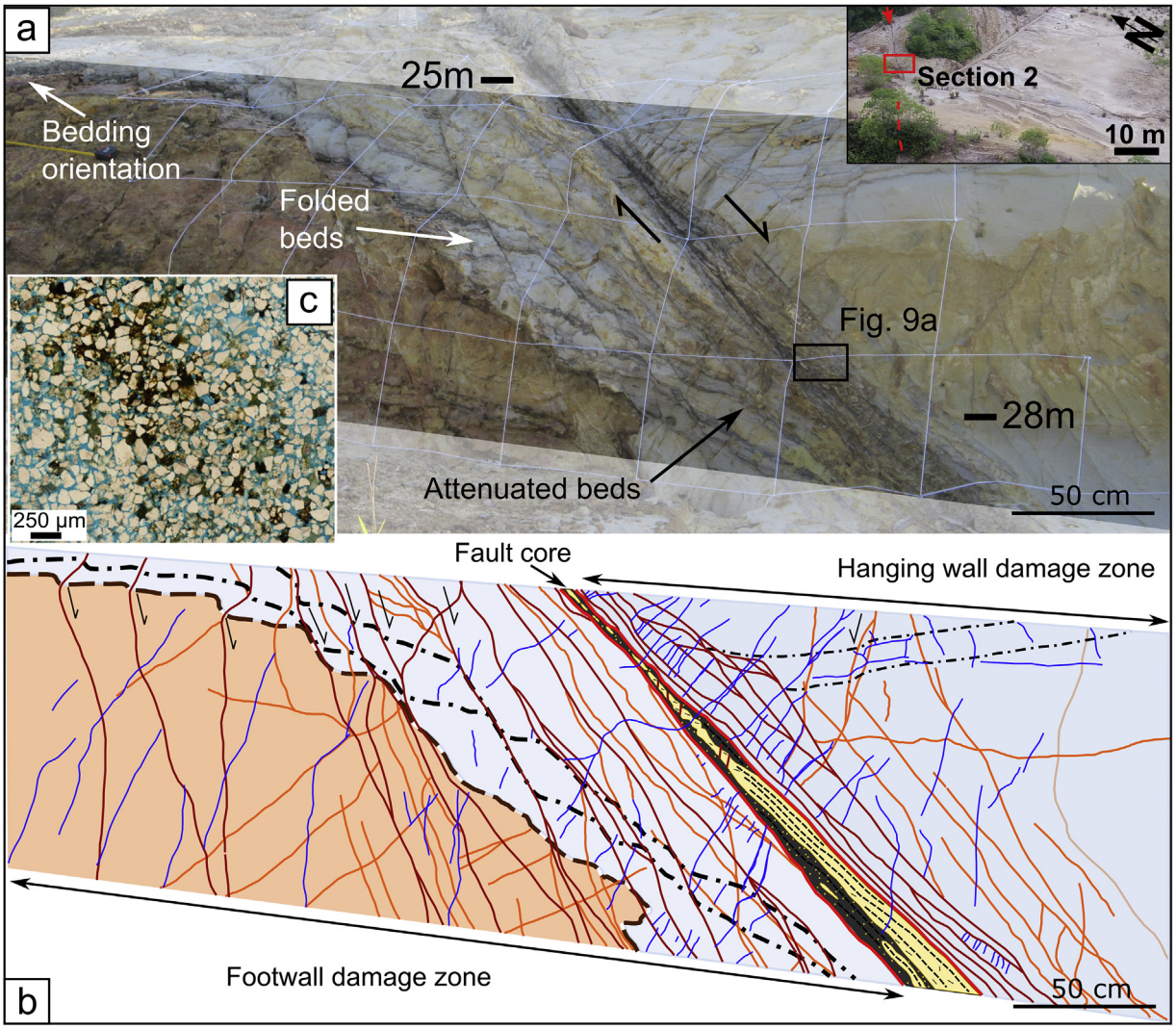

Fig. 4. Sub-vertical outcrop of the main fault, section 2. a) Picture showing footwall beds folded and attenuated towards the fault core through a set of shear zones and location of Fig. 9a is indicated. Inset shows location of section 2 on aerial photo. b) Map of the outcrop, see legend in Fig. 3 for reference. c) Plane-polarised-light photomicrograph of a deformation band cutting sand, impregnated with blue epoxy. Note the lack of cataclasis and the presence of Fe-oxide within the band (sample G6 on Fig. 2). (For interpretation of the references to colour in this figure legend, the reader is referred to the Web version of this article.)

footwall and hangingwall is grey sand with interlayered clay, silt and organic matter. For metres 0 to 1.5, the fault core composition is sand and silt (Fig. 3b), with slip surfaces bounding a cluster of anastomosing shear zones, stained by dark red iron oxides. The rest of the section has a foliated clay-rich fault core (Fig. 3c). Unfortunately a tree inside the fault core between metres 1.5 and 3 obscures the transition from sandy core to clay-rich core.

4.1.2. Section 2– Sub-vertical

Section 2 has a hangingwall composed of grey silty sand. The footwall is grey and orange sand separated by a hard iron-cemented horizon that does not follow the stratigraphy. These footwall beds are attenuated and gently curved towards the fault core through a set of normal shear zones separating rock volumes where the bedding is preserved, and gradually tilted in a stair-stepping geometry. The fault core is composed of foliated dark clay matrix and elongated white sand lenses (Figs. 2 and 4).

4.1.3. Section 3 – along strike

For section 3 between 29 and 32 m (Figs. 2 and 5), the clay-rich fault-core thickness increases, and the layered structure becomes less organised. The clay foliation and shear zones are wavy, and sand lenses are elongate parallel to the fault walls or to the internal shear zones. The foliation is absent from the fault core between 33 and 35 m where a chaotic assemblage of irregular sand lenses is present (Fig. 5b).

4.1.4. Section 4 – sub-vertical

Section 4 is partially oblique (metres 57–59) and partially sub-vertical (metre 59–60; Figs. 2 and 6). On the footwall side, grey and orange sands occur with the hard iron-cemented horizon in between, which can be traced to section 2, whereas hangingwall side comprises grey sand overlain by a clay bed. The clay-rich fault core thins and disappears between 59 and 60 m, being replaced by a breccia (fault breccia, as defined by Woodcock and Mort, 2008) composed of sand, silt, clay and organic matter rounded clasts in a sandy matrix.

4.1.5. Section 5– Along strike

Section 5 has a footwall composed of 20–30 cm clay beds interlayered with grey sands, while the hangingwall is grey sand. Layered clay smears are present on the footwall side (Figs. 2 and 7). Foliated clay and attenuated sand lenses form the fault core.

4.1.6. Section 6– Sub-vertical

Section 6 has a footwall with a 2 m-thick clay bed including

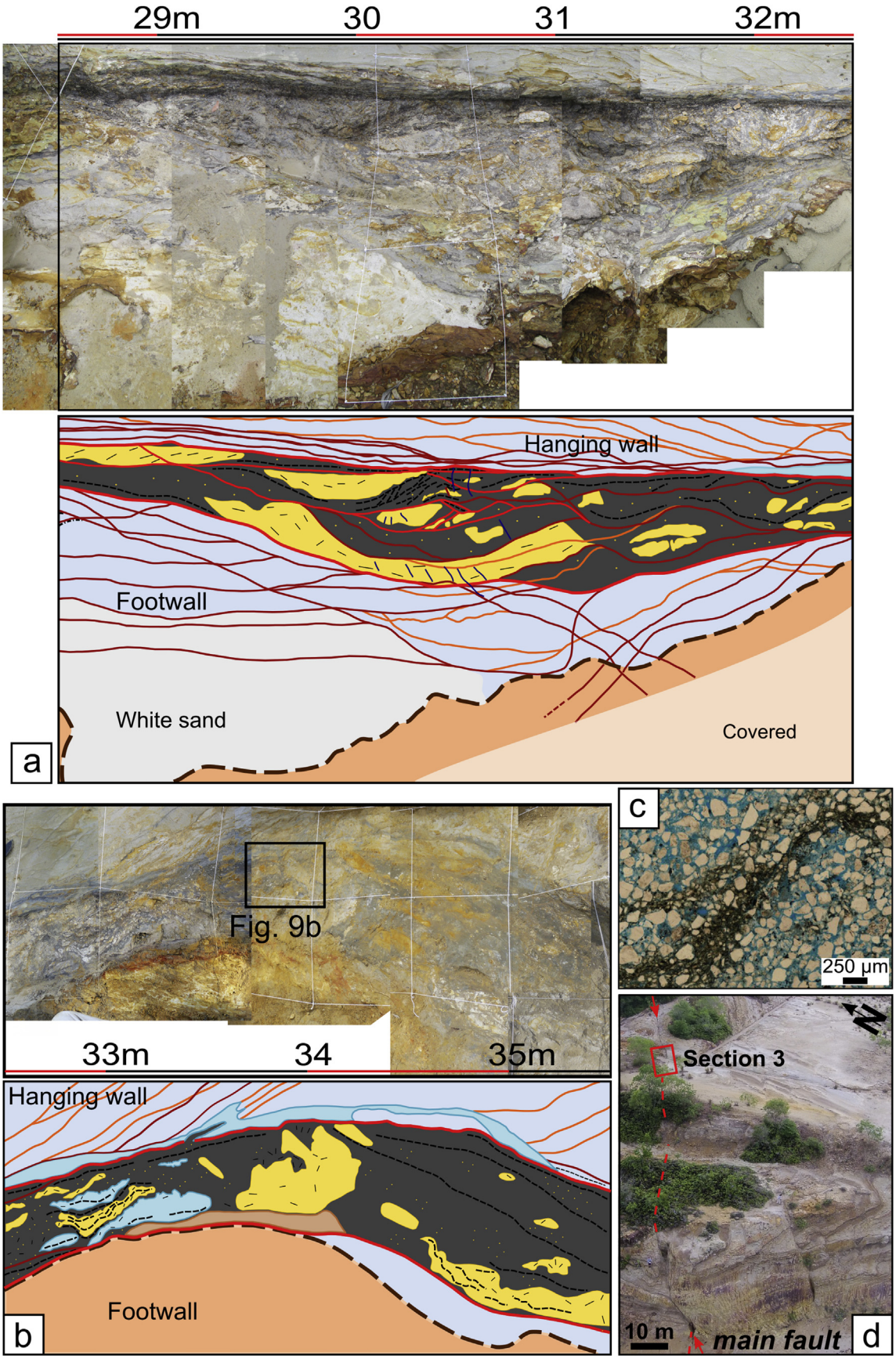

(caption on next page)

Fig. 5. Along-strike outcrop of main fault at section 3. a) Metres 29–32: the fault core becomes thicker and the foliation becomes wavy in comparison with sections 1 and 2. b) Excavated ditch, metres 32.5 to 35.5. The fault core becomes chaotic, and the wavy foliation is present only in small areas and location of Fig. 9b is indicated. See legend in Fig. 3 for reference. c) Plane-polarised-light photomicrograph of a shear zone cutting sand interlayered with clay, impregnated with blue epoxy (sample G5 on Fig. 2). d) Location of section 3 on aerial photo. (For interpretation of the references to colour in this figure legend, the reader is referred to the Web version of this article.)

interlaminated sand and silt, overlain by an orange sand bed (Figs. 2 and 8). These beds form clay and sand smear, respectively (Fig. 8). Grey sands form the hangingwall stratigraphy. The fault core is clay-rich and foliated.

4.2. Secondary faults FI and FII

The secondary faults FI and FII are being characterized because they provide information about core development in the host rock for small displacement faults. Two synthetic faults, FI and FII, offset the hangingwall of the main fault (Fig. 2a). FI outcrops are mostly along-strike,

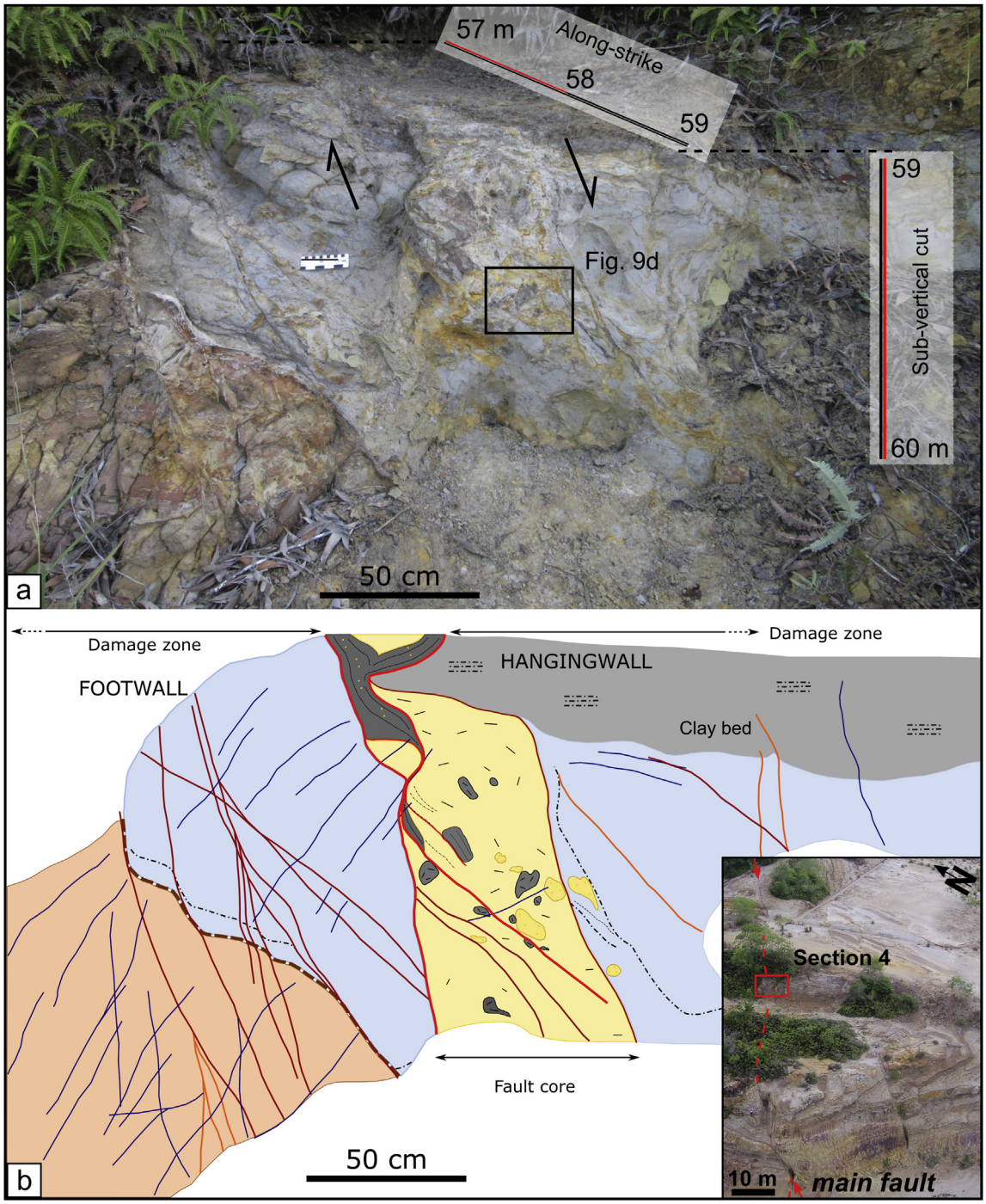

Fig. 6. Section 4: Sub-vertical outcrop in a small gully. Picture (a) and map (b) of the outcrop and location of Fig. 9d is indicated. Inset shows section 4 location on aerial picture. See legend in Fig. 3 for reference.

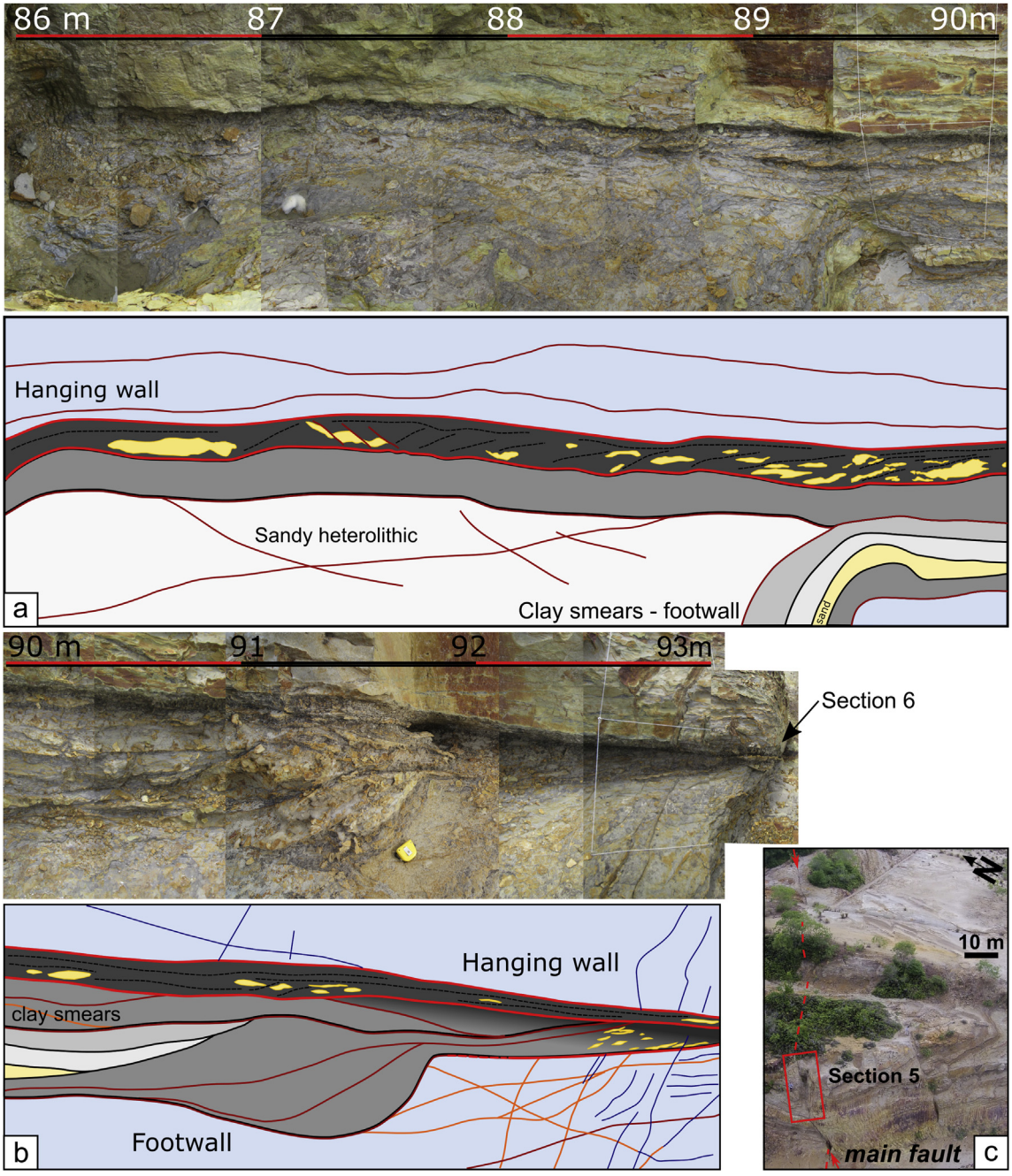

Fig. 7. Along-strike exposure of section 5: the footwall damage-zone topography is irregular, so only the area close to the fault core is mapped. a) Metres 86–90. b) Metres 90–93 with clay smears present on the footwall. See legend in Fig. 3 for reference. c) Location of section 3 on aerial photo.

and the offset increases from the SW towards the NE to a maximum of about 7.6 m, inferred from the offset of clay marker beds. FI dies out in a covered section just before the big cliff outcrop (section 6 of the main fault). FII throw increases in the opposite direction to FI. The maximum FII offset of 5.7 m is along the big cliff to the SW decreasing to 0.3 m in the NE. The FII fault plane dip varies between 60° and a maximum of 85° on the big cliff to the SW of the study area. Both faults have several minor strands.

The fault core of the secondary faults FI and FII have sand-rich core mainly toward their NE ends, while clay-rich core is prevalent to the SW. The sandy or sand and silt core consists of a cluster of anastomosing DBs if the offset of few decimetres, whereas the core is weakly foliated for offset greater than a metre. Foliation definition increases with clay content in these two subsidiary fault cores.

4.3. Microstructural analysis

From microstructural analysis, the dominant deformation mechanism is particulate flow with minor cataclasis. Particulate flow is defined as sliding and rolling of grains past each other (Borradaile, 1981). Deformation bands show very weak rearrangement of sand grains, and deposition of Fe-oxide along them in places (Fig. 4c). Conversely, the shear zones are characterized by sand and clay grain rotation and sliding (Fig. 5c). The clay-rich fault core is characterized by alignment of clay particles, which show maximum interference colours at the same angle (Fig. 8c).

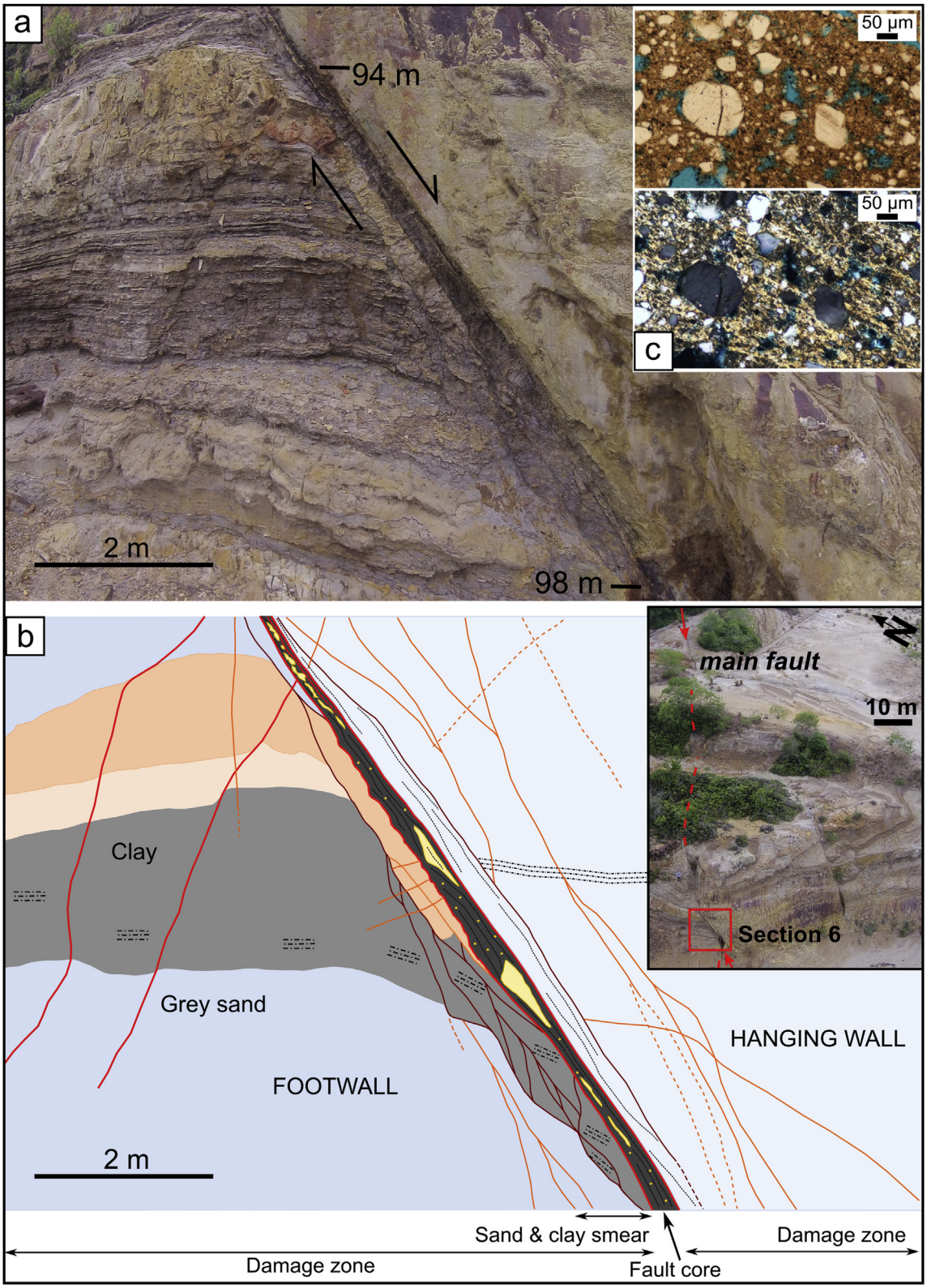

Fig. 8. Sub-vertical cut at the SW end of the main fault (big cliff, section 6). Picture (a) and map (b). Sand and clay smear originate from footwall beds. Inset shows location of section 6 on aerial photo. See legend in Fig. 3 for reference. c) Plane-polarised and cross-polarised light photomicrograph of foliated clay-rich fault core, impregnated with blue epoxy (sample G8 on Fig. 2). (For interpretation of the references to colour in this figure legend, the reader is referred to the Web version of this article.)

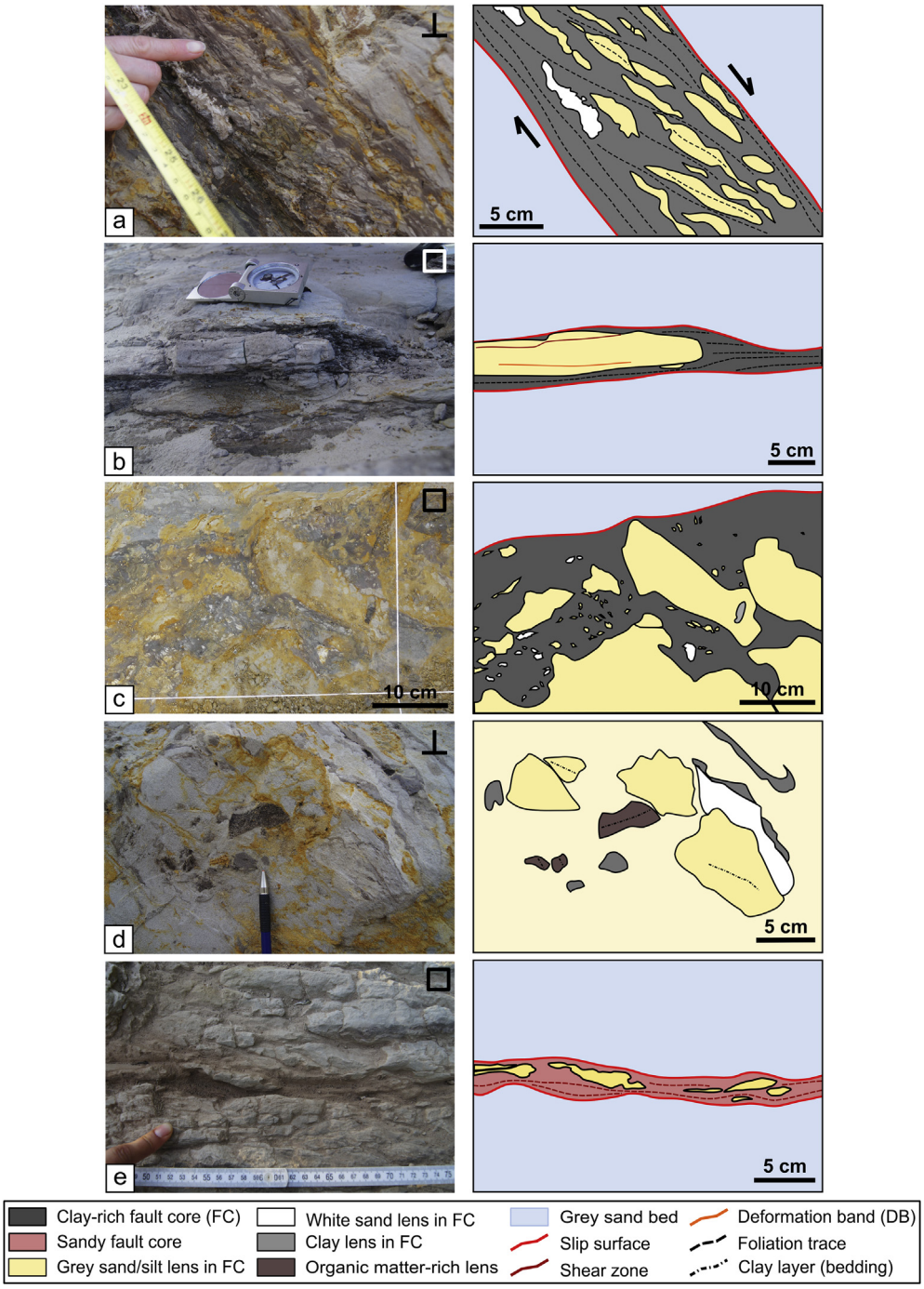

Fig. 9. Fault core types identified along the main fault, picture on the left and sketch on the right. a) Foliated clay-rich fault core and elongate sand lenses (section 2). b) Thin, foliated clay-rich fault core with sand lens in the middle (section 1). c) Chaotic clay-rich fault core with irregular sand lenses (section 3). d) Sandy breccia fault core with clasts of different composition and orientation (section 4). e) Anastomosing sandy and silty shear zone fault core, with weakly deformed sand lenses (section 1). Outcrop orientation: □ indicates plan view; ⊥ indicates sub-vertical view.

5. Main fault core architecture

At all sites, the main fault core is bounded by slip surfaces on both sides (Figs. 3–8). The hangingwall slip surface is generally straight and regular, while the footwall slip surface is curvy and in general less regular. Sand lenses within the fault core can be either white sand, or blue-grey silt and sand. The white sand is lighter in colour than the host rock, likely indicating bleaching. Five distinct types of fault core have been identified at the site:

a) **Foliated, clay-rich fault core** (2–35 cm thick) is the dominant fault core type found in all sections. The foliation is marked by compositional banding, alignment of clay minerals in a dark clay-rich matrix (pattern becomes visible upon drying) and by elongated sand lenses, and does not involve any macroscopic mineralogical change. Some sand lenses embedded in the clay matrix are boudinaged. Layers of the fault core can sometimes be identified by a slight difference in colour of the clay matrix, or by differences in the number, size and orientation of sand lenses (e.g. Fig. 9a).

b) **Thin, foliated clay-rich fault core** (1 mm-2 cm thick) occurs mostly at section 1, and at one location in section 5. The foliated clay-rich fault core thins out to 1–2 cm or two branches of a few mm

that enclose a sand lens (Fig. 9b). This type was identified because of its relevance to discussions about cross-fault fluid flow.

c) **Chaotic, clay-rich fault core** (30–60 cm thick) is found only at section 3. The chaotic core presents a less organised texture in comparison to the foliated core. The foliation is partly present on the hangingwall edge, while the rest of the fault core is dominated by chaotic pods of sand with wavy or irregular geometry floating in a clay matrix (Fig. 9c).

d) **Sandy breccia** (26–36 cm thick) is found only at section 4. It is composed of sand and clay clasts supported by a sandy matrix. The clasts are sub-angular to sub-rounded. Sand clasts are mainly grey sand and silt, but in places the sand is white. Sand clasts can be up to 10–20 cm in size. Clay clasts are generally smaller (few cm) and mostly sub-rounded. Some clay clasts are very rich in organic matter (Fig. 9d).

e) **Anastomosing sandy shear zones** (2–4 cm) occurs only at the top end of section 1. Here, the fault core is formed by a set of anastomosing shear zones. The shear zones are composed of sand and silt from the host rock, and dark red iron oxides. Between the shear zones there are elongated lenses of less deformed, and less eroded sand, generally a few cm long (Fig. 9e). It was not possible to collect an intact sample of this material to determine by microscopic examination the deformation mechanisms. Cataclastic deformation bands often have relatively high relief on outcrop surfaces, and reduced porosity in comparison with the host rock (Antonellini et al., 1994). In contrast, the sandy shear zones that we observe in the fault core are eroded more than the surrounding rocks. We interpret the relatively higher erosion and the presence of dark red iron oxides inside the sandy shear zones, but not in the surrounding sands or in the sand lenses, as an indication of enhanced shear zone permeability during or after fault displacement.

5.1. The geometry of internal shear zones

Shear zones inside the fault core develop on the edge of sand lenses and in the clay-rich matrix. The clay foliation and sand boudins define a Riedel-shear geometry, both in plan view and in vertical view. Y-shears are defined by the fault-core slip surfaces and parallel foliation. P-shears are evidenced by offset of the preserved bedding inside of the sand boudins, which were rotated, or by the elongation of the sand lenses themselves. R-shears displace the sand boudins and quickly die out in the clay matrix (Fig. 10a). In vertical cuts, the Riedel shears show a normal sense of displacement for the main faults, but along-strike they display a dextral component of displacement (Fig. 10b).

Minor, straight shear zones sometimes separate clays in the middle of the fault core from clays filling an irregularity in the fault plane. Clay filling the concavity usually shows a curved foliation, parallel to the concavity edges, while the rest of the clay-rich core shows planar foliation. This mechanism is observed both on the strike exposures of section 1 and 7 of the main fault, and along the synthetic faults FI and FII (see section 10). The length of the cut-off area is between 30 and 50 cm, and the thickness is generally a few cm (mean of 3.5 cm).

6. Fault core thickness along-strike

The clay-rich fault-core thickness of the main fault varies from 0 to 60 cm (Fig. 11a and d). The mean clay-rich fault core thickness is 16 cm. The foliated clay fault core occurs along 80.5% of the total mapped length of the main fault of which 2.7% (about 1.5 m) is the length of very thin (≤ 2 cm) clay-rich fault core (Fig. 11a, blue diamonds). The clay-rich, chaotic core is 16% of the total length of the main fault, while the total length of sand-on-sand juxtaposition is 3.5% of the main fault exposure (2 m).

FI fault core thickness varies between 1 mm and 25 cm, whereas FII core thickness is between 0.1 and 40 cm (Figs. 10b, 11c and 11e). These thickness measurements include sand lenses. Clay-rich fault core thickness histogram statistics for main fault and faults FI and FII are presented in Appendix 1.

Fig. 12a shows the main fault-core thickness variations along strike (as in Fig. 11a) and the relative fault-core type at each location where a thickness measurement was recorded. Anastomosing sandy shear zones (Fig. 12b) and attenuated, foliated clay core (Fig. 12c) constitute the thinner core areas. Thicker fault cores are composed of a chaotic clay-rich fault core (Fig. 12d), while the sandy breccia (Fig. 12e) has a comparable chaotic texture to the chaotic clay-rich core but is thinner. The rest of the outcrop for the main fault is dominated by the foliated clay-rich fault core (Fig. 12f).

The main fault-core thickness variations along-strike and down dip are not, at the scale of observation, related to the fault offset. In fact, the offset increase of about 5 m from the NE to the SW (from section 1 to section 7) is not coincident with any notable core thickness increase (Fig. 12a). Shipton et al. (2006) and Caine and Minor (2009) also failed to find a consistent correlation between the thickness of the fault core (or clay smear) and the displacement along-strike after a fault core becomes well established during deformation.

The fault core thickness seems to be only partly related to the nearby stratigraphy, in particular the footwall stratigraphy. At the locations where clay beds (20–200 cm thick) are incorporated from the footwall into the fault, core thickness generally increases. This increase is greater for a set of clay beds as opposed to a single bed. The core thickness then diminishes down dip as the distance from these source beds increases (section 5 and 6). However, the chaotic fault-core texture, which is present in the thickest fault core section, does not correlate with any marked change in the footwall stratigraphy.

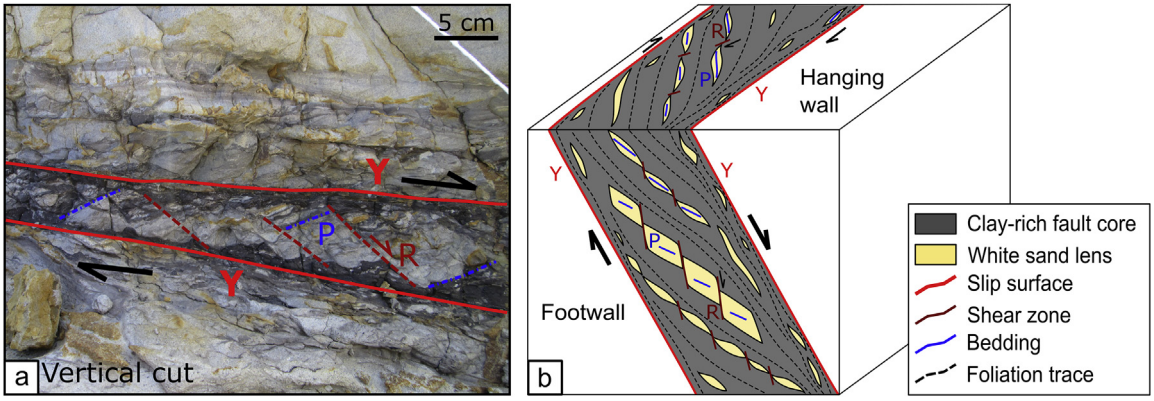

Fig. 10. Riedel shears evidenced by white sand lenses in the dark clay-rich matrix of the fault core. a) Fault core bounded by slip surfaces representing Y-shears, partly preserved bedding inside of the sand lenses along P-shears and synthetic R-shears displacing them (section 2, sub-vertical exposure). b) 3D diagram of the Riedel shears and related normal sense of movement along the main fault with minor dextral component.

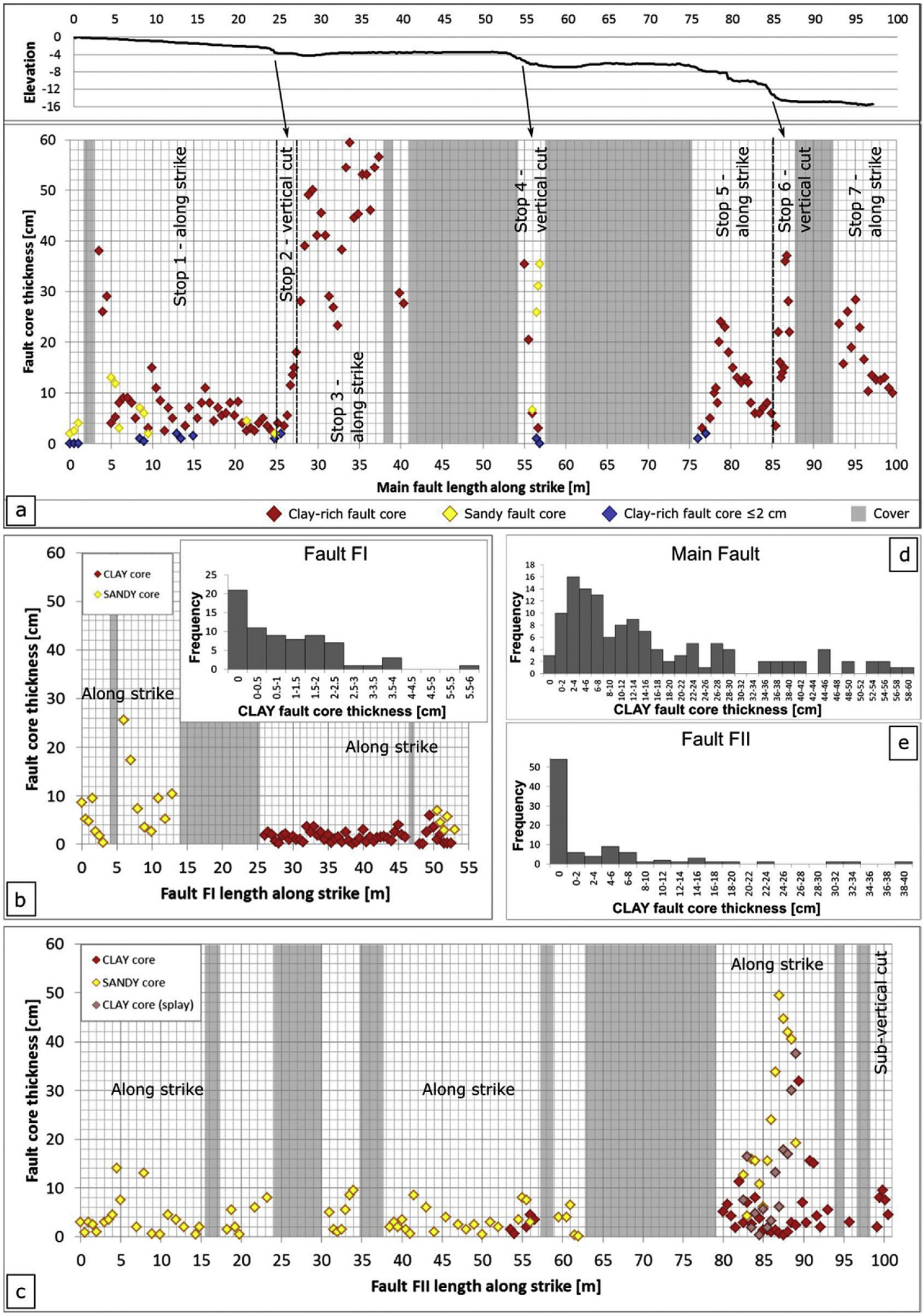

(caption on next page)

Fig. 11. Fault core thickness and composition variation along-strike. a) Main fault, with sections 1–7 indicated both in the graph and in the topographic profile on top. b) Secondary fault FI thickness variation along length and histogram of the clay-rich fault core thickness (all yellow diamonds correspond to zero clay-rich fault core thickness). c) Secondary fault FII thickness variation along length; d) and e) show main fault and FII clay-rich fault-core thickness histograms. See supplementary information for the histograms statistics in Appendix 1. (For interpretation of the references to colour in this figure legend, the reader is referred to the Web version of this article.)

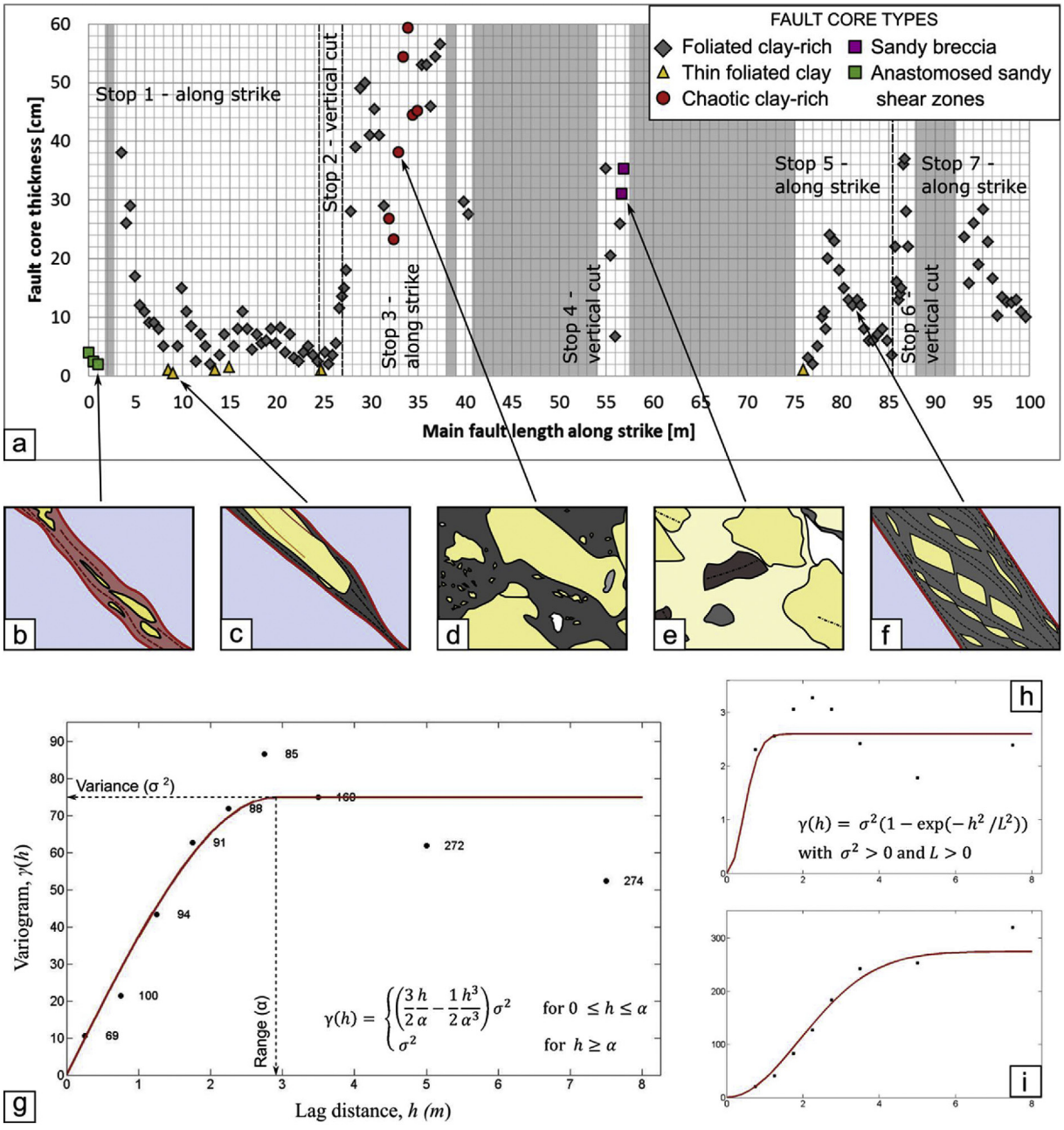

Fig. 12. Fault core types related to the fault core thickness along-strike. a) Main fault core thickness variation along strike, as in Fig. 10; a cartoon of each fault core type is related to the section where it is outcropping and to the fault core thickness at the specific location. b) Anastomosing sandy shear zones. c) Thin, foliated clay-rich fault core. d) Chaotic clay-rich. e) Sandy breccia. f) Foliated clay-rich. g) Experimental and theoretical variogram derived from the along-strike fault core thickness data in (a). The fitted variogram is for a spherical covariance distribution with a range of 2.9 and a variance of 75. h) and i) show the along-strike fault core thickness variograms for secondary faults FI and FII respectively. Both variograms are fitted with a Gaussian covariance distribution with a range of 1.3 and a variance of 2.6 (h), and a range of 4.5 and a variance of 275 (i); L is the distance at which 95% of the sill is reached; x- and y-axis are the same as in (g). Equations from: Kitanidis, 1997.

Thickness variations in the clay-rich fault core cannot simply be ascribed to stratigraphic variations. At this site, the clay and sand bed thicknesses are small in comparison to the likely offset on the main fault. Individual clay beds show some thickness variability, but they are continuous at the outcrop scale. Hence, the footwall and hangingwall stratigraphy that moved past each point on the fault, along the strike section, must be very similar and could not have been the cause of the large variability in fault core thickness.

Pore throats in clays are generally much smaller than in sand, therefore a much higher across-fault fluid pressure is needed to reach

the capillary entry pressure (Watts, 1987). Consequently, for predicting capillary barriers, it is important to understand the distribution of high permeability materials in the clay fault core. At this site, two sand-rich fault core types, anastomosing sandy shear zones and sandy breccia, occur and both are likely to have considerably lower pore entry pressures than the clay-rich fault cores, because of their bigger pore throat size. This behaviour means that such areas would be preferential pathways for across-fault fluid leakage, with the leakage rate determined both by the lateral and vertical extent of the patches of sandy fault core and by the frequency with which they occur within the fault plane. These observations underline the need for a mechanistic understanding of fault-core evolution so that the formation, frequency and size of such high-permeability areas in the fault core can be predicted.

When simulating reservoir flow in production scenarios, complex fault architectures must be up-scaled to provide a small number of simplified parameters for application at the scale of a reservoir simulator grid-cell. Using mean clay-rich fault-core thickness (16 cm) would poorly represent the hydraulic properties of this fault. This outcome is because geological material characteristics, such as fault-core thickness, are not truly random, they are spatially correlated, and it is predicting the patches of *thin* fault core that matters the most for hydraulic performance. In a spatially correlated field, a known value of fault-core thickness at one location on the fault makes it more likely for a neighbouring second location to be similar. This spatial correlation occurs up to a specific distance apart, called the correlation length, beyond which the value at the second location is entirely independent of the known value at the first. Visually, the correlation length is related to the size of 'thick' and 'thin' patches on the fault. The method for describing spatially correlated data is called a geostatistical variogram analysis (Matheron, 1971) and it has been used extensively to describe spatially varying geological properties such ore body percentage, porosity and permeability.

We performed a variogram analysis of fault-core thickness on the along-strike sections of the outcrop, using 0.5 m spaced thickness measurements. The variogram describes the square of the differences in fault thickness between pairs of data points (plotted on the y-axis) at a given distance apart (plotted on the x-axis). So, for locations on the fault that are very close together (small values on the x-axis) fault thickness is very similar (i.e. the difference in thickness between pairs of adjacent points is close to zero). Then, as the distance between points increases, the variogram value increases until it reaches a steady value, at which the pair of thickness values are unrelated, and hence equal to the background variance.

On the main fault, the experimental variogram is best fitted by a spherical covariance distribution which reaches a steady background variance at a distance of approximately 3 m (Fig. 12g.). This implies that 'patches' of thin and thick fault core are generally less than 3 m in length, termed the correlation length. Similar results as in Fig. 12g are obtained for the secondary faults FI and FII (Fig. 12h and i), however for them, a gaussian covariance distribution is a better fit to the experimental data. The spacing between measured data points (0.5 m) may be too large to capture the fault-core thickness variations of fault FI (Fig. 12h), which would explain the lack of data between 0 and 1 m on the experimental variogram. The occurrence of along-strike spatially correlated variations in clay-rich fault-core horizontal thickness at the < 3 m scale in the secondary faults FI and FII as well as in the main fault means that the processes responsible for creating a system where the significant changes in core thickness occur about every 3 m must already be active at an early stage of fault evolution (offset 1–10 m). Consequently, these fitted variogram functions can be used to generate faults with realistic fault-core thickness variations along strike.

The observed spatial correlation (Fig. 12g) in along-strike core thickness at the 0.5–3 m scale, alongside seemingly uncorrelated, but highly variable fault thickness and composition at a > 3 m scale, implies the superposition of at least two very different processes that contribute to fault zone variability that will be discussed in sections 7.2 and 7.3.

A correlation length of 3 m may be related to fault geometry and layer thickness, and other sites may contain thickness variations at a different scale. Lunn et al. (2008) calculated a correlation length for fault core thickness of 1.45 m for the Big Hole fault in aeolian sandstones (Utah). Responsible factors could also include the degree of host rock consolidation, host rock composition, stratigraphic variations, stress state and deformation history.

7. Discussion

7.1. Fault growth and clay smearing

The studied outcrops offer a rare opportunity for fault evolution analysis to be investigated in soft sediments in 3D. Fault offsets at the Jalan Mukah outcrop range from centimetre, to metre scale (secondary faults FI and FII) to the tens of metre scale (main fault). Using greater offset as a proxy for longer duration of fault evolution, we propose this structural evolution:

- Incipient deformation occurred through the formation of deformation bands and shear zones. Shear zones formed in mixed sand-clay sediments at offsets of a few cm, up to 1 m. Often, a shear zone was composed of several strands of minor shears or deformation bands, but no clear fault core-damage zone distinction was present. The host rock maintained cohesion across the deformed volume of rock, and no slip surfaces or fractures formed. The deformation bands display a large range of orientations with variations in strike and dip of up to 50° and shear zones vary in orientation for strike by up to 15° and dip by up to 45°, as the deformation is not well localised.
- At offsets between 1 and 10 m, the fault core-damage zone started to form, however it was not yet well established. The fault became simply composed of anastomosing shear zones. Fault core thickness of a single strand was generally between 1 and 10 cm with a maximum observed thickness of 40 cm. Faults were composed of one or more strands, and several segments linked together. At this stage of evolution, one or two slip surfaces localised at the edge of the fault core. A single slip surface can be located on either side of the clay or sand-rich fault core or cut across it. As the displacement increased from less than 1 m to few m, the slip surface orientations become more similar, indicating a greater degree of deformation localisation. The fault-core internal structure is generally weakly foliated to foliated, commonly with fault-bounded sand lenses. Clay smears are observed deflecting into the fault both from hangingwall and footwall stratigraphy. These observations are consistent with Van der Zee and Urai (2005), who studied dip-slip exposures of normal faults with throws up to 10 m at the Airport Rd outcrop in the same sedimentary sequence of the Jalan Mukah site. They reported a foliated structure of sheared clay with sand in the fault core, locally originating from thinly layered sand-clay beds. They also observed that most faults formed by several non-co-planar segments linking together so that increasing offset caused a strongly variable fault zone thickness.
- For offset between 10 and 50 m, the fault core-damage zone architecture became well established, but the thickness of both fault core and damage zone was quite variable. The fault core is bounded by slip surfaces on both sides. The hangingwall slip surface is straighter and more regular than the footwall slip surface, which is generally corrugated at the decimetre-to metre-scale. As the deformation localised, the orientation of the main fault became less variable (variation in strike of up to 19° and dip of up to 17°, hangingwall slip surface) than the smaller-offset faults. A foliated-clay structure developed in most of the clay-rich fault core.

Several authors (Heynekamp et al., 1999; Sigda et al., 1999; Rawling et al., 2001, 2003; 2006; Caine and Minor, 2009; Balsamo

et al., 2010; Loveless et al., 2011) have noted the presence of mixed zones along faults in poorly consolidated sediments. These studies are in poorly consolidated siliciclastic units with grain size ranging from gravel to clay that underwent deformation through particulate flow at less than 1 km depth. These authors define mixed zones as being composed of tectonically mixed material from either side of the fault, and having a contrasting permeability distribution that varies widely between the host rock sand and the fault core values (Sigda et al., 1999). The sandy breccia observed at the study site could represent a mixed zone from the textural point of view. However, it is located between the hangingwall and footwall damage zones, and the fault zone lacks other structural features. Therefore, it has to represent the part of the fault zone where the maximum displacement is accommodated. Heynekamp et al. (1999); Sigda et al. (1999); Rawling et al. (2001) and Rawling and Goodwin (2003) defined the mixed zone as being located between the fault core and the damage zone rather than being the fault core. Loveless et al. (2011) considers the mixed zone as representing the fault core based on hydrological behaviour. Due to this ambiguity in the meaning of the term mixed zone, we prefer to use the term breccia as a geometrical description of the sandy pods texture.

7.2. Variations in fault wall geometry

Smooth variation in fault thickness could be explained by fault-wall topography. It is well-known that fault-wall topography affects the thickness of the fault core (Lindsay et al., 1993). A fault-wall asperity is likely to be abraded away as displacement increases and the fault core develops. The abrasion of a sand body from one of the fault walls may also result in the increase of sand in the fault core system in the form of sand lenses. However, if a relatively hard volume of sand extrudes from either the footwall, the hangingwall or both, towards the fault core, it could cause an interruption of the clay smear instead of being abraded away. In this case, the clay smear would be squeezed outwards from the extruding fault walls, and the clay-rich fault core would be replaced by anastomosing sandy shear zones.

By contrast, if a fault wall contains a concavity, it can be filled by clay from the fault core. At several locations, we observe planar shear zones that separate clay within an irregularity in the fault plane, where the clay was derived from the fault core. Clay filling a concavity usually displays a curved foliation parallel to the surface of the concavity wall (Fig. 13a). This geometry is observed both at the study site for displacements at the metre- (FI and FII) to tens of metre-scale faults (main fault), and for other clay-rich fault cores (Cowan et al., 2003; Kremer et al., 2018). The curved slip surface of this structure has a similar geometry to the sidewall ripout mechanism of Swanson (1989). He observed asymmetric sidewall ripouts in pseudotachylite-bearing strike-slip faults in metamorphic rocks, and attributed them to adhesion wear between fault walls. The main differences are the host rock types and the fact that we do not observe a systematic asymmetry in the geometry of the curved slip surface.

Considering a schematic model for developing sidewall rip-outs, the clay-filled concavity is likely to develop where the host rock is composed of softer material, as compared to the rest of the fault wall (Fig. 13b). We suggest that during fault movement, clay in the fault core began to abrade and incorporate this softer material. It is likely that the clay from the fault core was pushed and smeared laterally in the concavity and downward by the fault movement. Clay platelets and sand lenses deforming through particulate flow probably adhered to the concavity walls forming a curved compositional banding and clay foliation within the concavity (Fig. 13c). Increasing deformation possibly determined the formation of a straight shear zone or slip surface cutting off the lobe-shaped concavity from the fault core, maybe favoured by a relatively faster movement along the fault plane (Fig. 13d). This abandonment of the clay inside the concavity reduces the overall volume of clay in the active part of the fault core system.

7.3. Disruptive fault evolution processes

The thickest fault core is associated with the chaotic clay-rich core. Therefore, three key observations must be explained: 1) the transition from well organised, foliated fault core to chaotic fault core happens in a relatively short distance (2–3 metres) along strike; 2) this transition is not matched by any observable lithological changes in the wall rock or degree of lithification; and 3) the transition is not associated with a geometric variation in the fault plane. It is possible that the chaotic breccia formed by the same processes that formed reported examples of “mixed zones”. Authors that have reported mixed zones describe that these textures are usually formed by disaggregation and penetrative particulate flow under low confining stresses. Rawling and Goodwin (2006) speculated that faults form with a stair-stepping geometry in lithologically layered sequences and that smoothing of these surfaces results in the generation of the mixed zone. They argued that the fault core subsequently localised within the centre of this zone because it is weaker than the surrounding rocks. However, this explanation and geometry do not match our observations in Miri. If this mechanism was responsible for the formation of a mixed zone, we would expect it to occur at all positions along fault strike, because the controlling mechanical variations in the stratigraphy are uniform along the fault trace. However, we have a discrete occurrence of the chaotic core, and so must invoke mechanisms that are localised. Three possible scenarios are proposed:

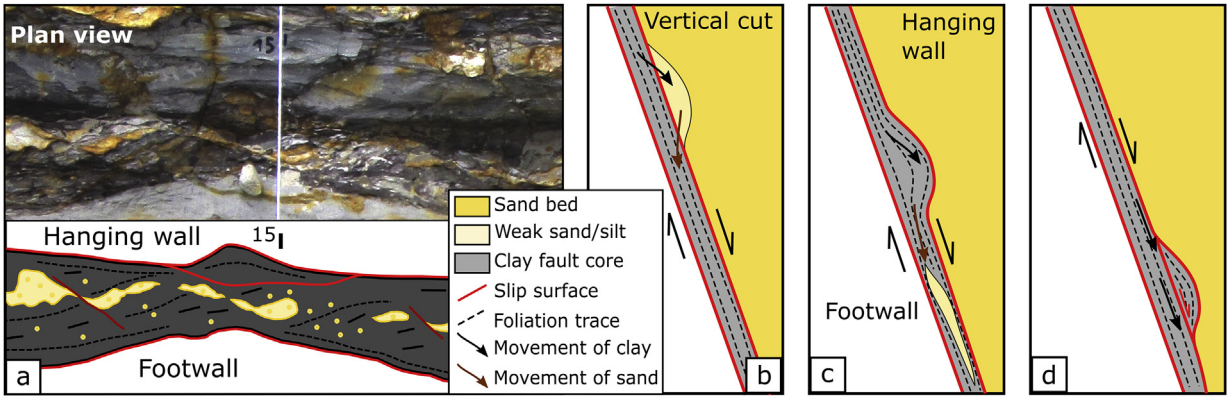

Fig. 13. Field example and cartoon of the sidewall ripout mechanism. a) Picture (top) and map (bottom) of an along-strike section of section 1; Cartoon: a weaker area on the hanging wall (b) is eroded away and incorporated as a sand lens (c) as the space is filled by foliated clay. d) The infill-area is subsequently cut-off from the main fault core by a straighter slip surface or shear zone.

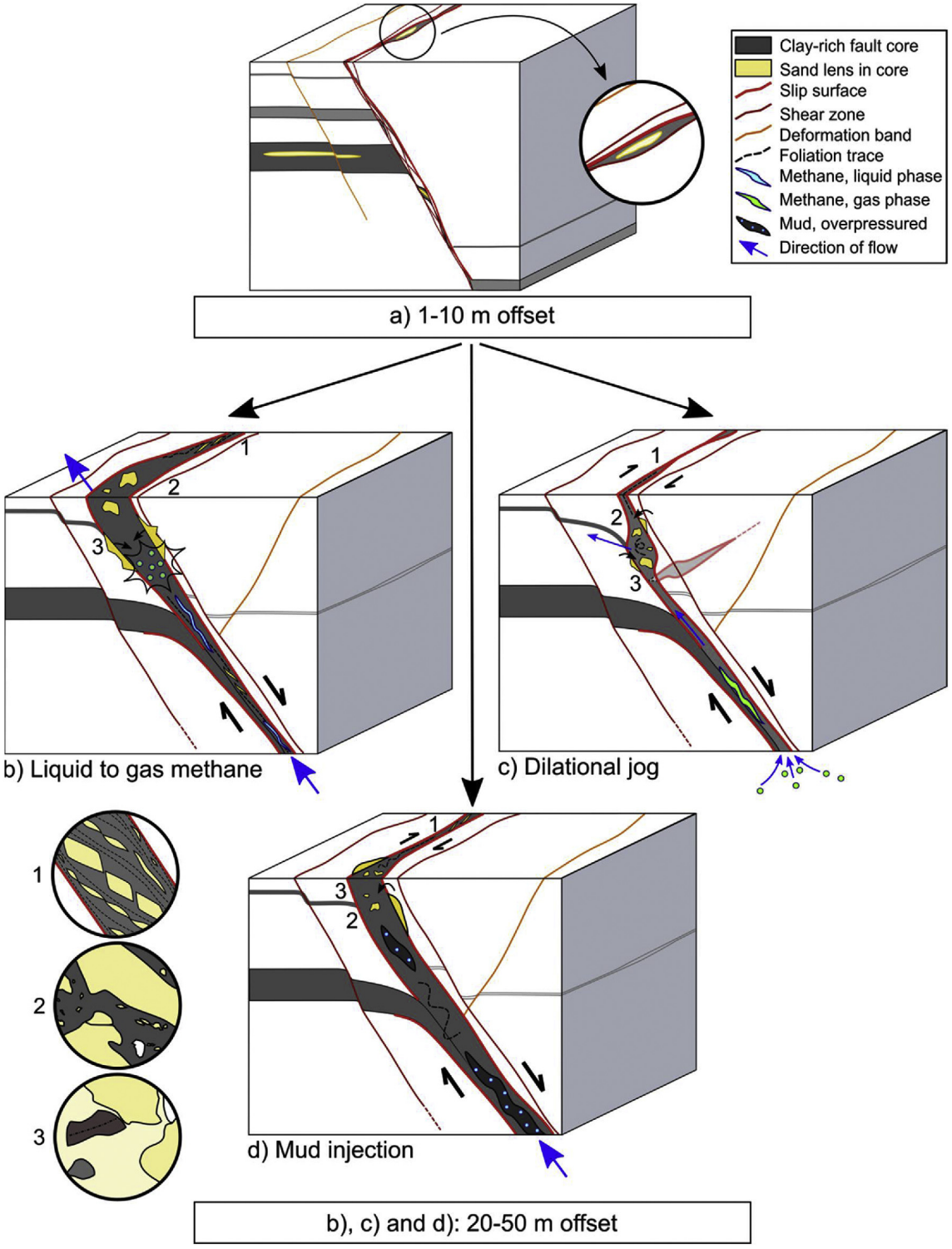

Fig. 14. Schematic fault evolution at Jalan Mukah outcrop. a) At 1-10 m offset the fault core begins to form, there is clay smearing from both hanging wall and footwall, and the principal slip surface can be replaced by a secondary slip (inset); b, c and d are three possible evolution of stage a) to an offset between 20 and 50 m, that can explain the different fault core (FC) types observed in the main fault (1- Foliated clay-rich FC; 2- Chaotic clay-rich FC; 3- Sandy breccia FC). b) Upward flow of natural gas at the liquid state during faulting, and passage from liquid to gas phase. c) A coalescence of gas bubbles at depth is attracted into an almost instantaneous dilational jog during faulting. d) Overpressured clays from deeper beds are injected along the fault plane during deformation.

7.3.1. Syn-faulting upward migration of buoyant methane from deep sediments towards the seabed

In this first scenario, the pressure drop due to the decrease in depth as the fluid rises would result in a phase change from liquid to gas, with a related increase in volume (Fig. 14b). The gas expansion within the fault walls could induce erosion of fault wall material and incorporation into the core. The eroded material could be either incorporated into the fault as randomly oriented lumps of sand, accounting for the chaotic structure of the clay-rich fault core, or as an increased amount of dis-aggregated sand filling the core from footwall to hangingwall. In the

sandy breccia fault-core type, sub-rounded clasts of host rock (sand, sand and silt, clay and organic matter-rich beds) with partly preserved bedding are enclosed in the disaggregated sand material. Vertical migration of oil and gas along seismically resolvable faults has been described by Haney et al. (2005) and Cartwright et al. (2007). In the West Baram Delta system, hydrocarbon flow along faults has been reported by Sandal (1996), Laird and Morley (2011) and Algar (2012). The exsolution process of gas bubbles from saturated CH_4 brines is illustrated by Busch and Kampman (in press). They describe the formation of a free-gas phase in brines, which migrates up fractures when the dissolved gas saturation exceeds the saturation limits. This process is driven by a reduction in CH_4 solubility with decreasing hydrostatic pressure. Further, the velocity of the gas bubbles increases considerably with decreasing depth (Busch and Kampman, in press). This process is driven by a phase change occurring local to the fault rocks.

Vitrinite reflectance data from Schmitz et al. (2003) show a maximum burial depth of less than 1000 m for the Airport Rd sediments (the same unit of the study site). The temperature gradient reported for the Baram Delta is between 25 and 36 °C (Sandal, 1996; Tan et al., 1999; Madon, 1999). Morley et al. (2008) report a vertical stress gradient of 19–22 MPa/km at 1500 m below sea level for offshore Baram Delta Province. According to Ahmed (1989), pure methane at 25–30 °C intersects the vapor-pressure curve (bubble point) at pressures of 29–32 MPa. These pressures would be too high for the phase change to happen at 1000 m of depth. However, natural gas is a mixture of hydrocarbon components, and the overall physical and chemical properties depend on the individual components of the mixture and vary widely with the composition of the gas (Ahmed, 1989). Therefore, if the faults we studied were under the same temperature and stress gradient described by Sandal (1996) and Morley et al. (2008) they could have been at or close to the bubble point at the time of faulting.

7.3.2. Rapid opening of a dilational jog

In this second scenario, a dilational jog forms during a rapid slip event, and the opening collapses almost instantaneously due to the poorly consolidated sediments, creating a chaotic fault core fabric (Fig. 14c). A similar process was invoked by Woodcock et al. (2006, 2014) for the slow collapse of dilational cavities in hard rocks. In poorly consolidated rocks, such collapse would be immediate as they are so much weaker than the rocks examined by Woodcock. The transient pressure drop at such dilational cavities could further enhance disruption, sucking in local fluids (Sibson, 2000), perhaps accompanied by a phase change to gas. As these fluids transit through the core, they would disrupt the foliated clay-rich fault core structure, which is the dominant texture along the rest of the fault. What is left behind would be a more randomly-oriented clay matrix and irregular sand lenses. In a normal fault, a dilational jog would ideally form a sub-horizontal elongated opening. However, the dextral component of shear, demonstrated by the internal structure of Riedel shears in the along-strike exposures, could imply a slightly oblique conduit, able to channel the gas upwards.

7.3.3. The presence of a locally overpressured clay bed deeper in the faulted sequence

The final scenario is that a locally overpressured clay bed becomes mobilised as it is entrained into the fault (Fig. 14d). The clays would probably undergo rapid chaotic rearrangement during pressure release as they are entrained into the fault core, possibly eroding sand from fault walls (stoping) in the process. Such clay injection could explain both the structure of the chaotic fault core and the along-strike increase in fault core thickness. Parts of the foliated clay-rich core texture are preserved towards the edges of the fault core as wavy foliated-areas. This interpretation is supported by the fact that shale diapirs and pipes are common features in the West Baram Delta province (Sandal, 1996; and Morley et al., 2003), and Sandal (1996) reports injection of clay along faults as well. The overpressures responsible for such features are ascribed to undercompaction of clay units in the Baram Delta region, possibly combined with folding and inversion during the generation of hydrocarbons, particularly the cracking of oil to gas (Morley et al., 2008).

A degree of interplay exists between these three proposed scenarios. In fact, a dilational jog could attract not only a coalesced gas accumulation, but also gas in liquid phase or mobilised plastic clays. All three mechanisms could result in the erosion of fault walls. Bleaching of sand lenses inside the clay-rich fault core, as observed at the field site, is more likely in the first two scenarios, because hydrocarbons are a recognised agent for iron bleaching (Chan et al., 2000; Beitler et al., 2003; Parry et al., 2009).

All three of the scenarios discussed above invoke isolated sporadic occurrences of an abrupt disruptive process. As observed within the chaotic breccias, such processes are not likely to be spatially correlated. Hence, the fault core thickness is well-modelled by a continuous spatially correlated random field that has been overprinted and disrupted in short sections at sporadic locations. Future research will be required to estimate the spatial frequency and distribution of these sporadic events.

8. Conclusions

The Jalan Mukah outcrop offers excellent 3D exposures of a normal fault with 20–50 m offset. The fault core is exposed along-strike for 55 m. Five fault core types were identified. The fault core is generally comprised of continuous, low-permeability foliated clay which, where present, varies from 60 cm thick to a veneer of 1–2 cm. At some locations, the clay-rich fault core loses its foliated structure and becomes chaotic. Two sections of the fault core are sand-dominated: composed entirely of anastomosing sandy shear zones or of a sandy breccia. These sections represent high-permeability zones in the otherwise low-permeability clay-rich fault core.

Two (or more) processes appear to govern the along-strike fault core variability: one that controls the thickness in clay-rich fault core; and one (or more) that results in abrupt changes in both fault core thickness and composition. Controls on the thickness in clay-rich fault core could include the geometry, layer thickness, degree of host rock consolidation, host rock composition, stratigraphic variations, stress state and deformation history. To characterize these variations we used spatial statistics. The variogram of along-strike clay-rich fault core thickness has a spatial covariance with a correlation length of 3 m, that implies ‘patches’ of thin and thick fault core are generally less than 3 m in length.

Abrupt variations in fault-core composition and geometry could be explained by the occurrence of disruptive processes. We speculate that such processes could include rapid degassing, slip events opening voids, or sudden release of overpressure. Further investigation of faults in similar geological settings is needed to obtain a better understanding of the deformation processes acting at different scales that determine fault core thickness and composition variations, and therefore the relative changes in capillary pressure and sealing ability of the fault rocks.

Acknowledgements

This paper contains work conducted during a PhD study undertaken as part of the Natural Environment Research Council (NERC) Centre for Doctoral Training (CDT) in Oil & Gas [grant number NE/M00578X/1] and the University of Strathclyde Faculty of Engineering PhD Scholarships (SSDR), and NERC grant NE/N015908/1 (YK), whose support is gratefully acknowledged. We thank Fabrizio Balsamo, William Dunne and an anonymous reviewer for their positive and constructive comments.

Appendix A. Supplementary data

Supplementary data related to this article can be found at https://doi.org/10.1016/j.jsg.2018.08.012.

References

Ahmed, T., 1989. Hydrocarbon Phase Behaviour. Gulf Publishing Company, Texas 424 pp.

Algar, S., 2012. Big oil from "Gas-Prone" source rocks and leaking traps: northwest Borneo. AAPG Search Discov. 10465, 40.

Aydin, A., 2000. Fractures, faults, and hydrocarbon entrapment, migration and flow. Mar. Petrol. Geol. 17, 797–814. https://doi.org/10.1016/S0264-8172(00)00020-9.

Antonellini, M.A., Aydin, A., Pollard, D.D., 1994. Microstructure of deformation bands in porous sandstones at Arches National Park, Utah. J. Struct. Geol. 16, 941–959. https://doi.org/10.1016/0191-8141(94)90077-9.

Balsamo, F., Storti, F., Salvini, F., Silva, A.T., Lima, C.C., 2010. Structural and petrophysical evolution of extensional fault zones in low-porosity, poorly lithified sandstones of the Barreiras Formation, NE Brazil. J. Struct. Geol. 32, 1806–1826. https://doi.org/10.1016/j.jsg.2009.10.010.

Beitler, B., Chan, M.A., Parry, W.T., 2003. Bleaching of jurassic Navajo sandstone on Colorado plateau laramide highs: evidence of exhumed hydrocarbon supergiants? Geology 31, 1041–1044. https://doi.org/10.1130/G19794.1.

Borradaile, G.J., 1981. Particulate flow of rock and the formation of cleavage. Tectonophysics 72, 305–321. https://doi.org/10.1016/0040-1951(81)90243-2.

Burhannudinnur, M., Morley, C.K., 1997. Anatomy of growth fault zones in poorly lithified sandstones and shales: implications for reservoir studies and seismic interpretations: part 1, outcrop study. Petrol. Geosci. 3, 211–224.

Bretan, P., Yielding, G., Jones, H., 2003. Using calibrated shale gouge ratio to estimate hydrocarbon column heights. AAPG Bull. 87, 397–413. https://doi.org/10.1306/08010201128.

Busch, A., Kampman, N. (Accepted/In press), Migration and leakage of CO_2 from deep geological storage sites. In: Vialle, S., Carey, J. W., Ajo-Franklin, J. B. (Eds.), Caprock Integrity in Geological Caprock Storage (AGU Books), American Geophysical Union.

Caine, J.S., Evans, J.P., Forster, C.B., 1996. Fault zone architecture and permeability structure. Geology 24, 1025–1028.

Caine, J.S., Minor, S.A., 2009. Structural and geochemical characteristics of faulted sediments and inferences on the role of water in deformation, Rio Grande Rift, New Mexico. Bull. Geol. Soc. Am. 121, 1325–1340. https://doi.org/10.1130/B26164.1.

Cartwright, J., Huuse, M., Aplin, A., 2007. Seal bypass systems. AAPG Bull. 91, 1141–1166. https://doi.org/10.1306/04090705181.

Chan, M.A., Parry, W.T., Bowman, J.R., 2000. Diagenetic hematite and manganese oxides and fault-related fluid flow in Jurassic sandstones, Southeastern Utah. AAPG Bull. 84, 1281–1310. https://doi.org/10.1306/A9673E82-1738-11D7-8645000102C1865D.

Childs, C., Walsh, J.J., Manzocchi, T., Strand, J., Nicol, A., Tomasso, M., Schopfer, M.P.J., Aplin, A.C., 2007. Definition of a fault permeability predictor from outcrop studies of a faulted turbidite sequence, Taranaki, New Zealand. Geol. Soc. Lond. Spec. Publ. 292, 235–258. https://doi.org/10.1144/SP292.14.

Cowan, D.S., Cladouhos, T.T., Morgan, J.K., 2003. Structural geology and kinematic history of rocks formed along low - angle normal faults, Death Valley, California. Geol. Soc. Am. Bull. 115, 1230–1248. https://doi.org/10.1130/B25245.1.

Doughty, P.T., 2003. Clay smear seals and fault sealing potential of an exhumed growth fault, Rio Grande rift, New Mexico. AAPG Bull. 87, 427–444. https://doi.org/10.1306/10010201130.

Douglas, M., Clark, I.D., Raven, K., Bottomley, D., 2000. Groundwater mixing dynamics at a Canadian Shield mine. J. Hydrol. 235, 88–103. https://doi.org/10.1016/S0022-1694(00)00265-1.

Faerseth, R.B., 2006. Shale smear along large faults: continuity of smear and the fault seal capacity. J. Geol. Soc. 163, 741–751. https://doi.org/10.1144/0016-76492005-162.

Faulkner, D.R., Jackson, C.A.L., Lunn, R.J., Schlische, R.W., Shipton, Z.K., Wibberley, C.A.J., Withjack, M.O., 2010. A review of recent developments concerning the structure, mechanics and fluid flow properties of fault zones. J. Struct. Geol. 32, 1557–1575. https://doi.org/10.1016/j.jsg.2010.06.009.

Haney, M.M., Snieder, R., Sheiman, J., Losh, S., 2005. A moving fluid pulse in a fault zone. Nature 437, 46. https://doi.org/doi:10.1038/437046a.

Heynekamp, M.R., Goodwin, L.B., Mozley, P.S., Haneberg, W.C., 1999. Controls on fault-zone architecture in poorly lithified sediments, Rio Grande rift, New Mexico: implications for fault-Zone permeability and fluid flow. Faults Subsurf. Fluid Flow Shallow Crust 27–49. https://doi.org/10.1029/GM113p0027.

Hutchinson, C.S., 2005. Geology of North West Borneo: Sarawak, Brunei and Sabah. Elsevier, New York, USA 421pp.

Kessler, F., Jong, J., 2017. Examples of fault architecture and clay gouging in Neogene clastics of the Miri area, Sarawak clastics of the Miri area, Sarawak. Warta Geol. 43 (1), 15–20.

Kettermann, M., Thronberens, S., Juarez, O., Urai, J.L., Ziegler, M., Asmus, S., Krüger, U., 2016. Mechanisms of clay smear formation in unconsolidated sediments-insights from 3-D observations of excavated normal faults. Solid Earth 7, 789–815. https://doi.org/10.5194/se-7-789-2016.

Kitanidis, P.K., 1997. Introduction to Geostatistics. Cambridge University Press, Cambridge, pp. 249.

Kremer, Y., Shipton, Z.K., Lunn, R.J., Sosio de Rosa, S., 2018. What's inside a fault? Architecture and composition of faults in sand-shale-silt sequences. Am. Assoc. Petrol. Geol (in press).

Laird, A.P., Morley, C.K., 2011. Development of gas hydrates in a deep-water anticline based on attribute analysis from three-dimensional seismic data. Geosphere 7, 240–259. https://doi.org/10.1130/GES00598.1.

Lehner, F.K., Pilaar, W.F., 1997. The emplacement of clay smear in synsedimentary normal faults: inferences from field observations near Frechen, Germany. In: In: Møller-Pedersen, P., Koestler, A.G. (Eds.), Norwegian Petroleum Society Special Publications: Hydrocarbon Seals Importance for Exploration and Production, vol. 7. Elsevier, Singapore, pp. 39–50. https://doi.org/10.1016/S0928-8937(97)80005-7.

Lindsay, N.G., Murphy, F.C., Walsh, J.J., Watterson, J., 1993. Outcrop studies of shale smears on fault surfaces. Spec. Publ. Int. Assoc. Sedimentol. 15, 113–123.

Loveless, S., Bense, V., Turner, J., 2011. Fault architecture and deformation processes within poorly lithified rift sediments, Central Greece. J. Struct. Geol. 33, 1554–1568. https://doi.org/10.1016/j.jsg.2011.09.008.

Lunn, R.J., Shipton, Z.K., Bright, A., 2008. How can we improve estimates of bulk fault zone hydraulic properties? The Internal Structure of Fault Zones: implications for mechanical and fluid-flow properties. Geol. Soc. Lond. Spec. Publ. 299, 231–237. https://doi.org/10.1144/SP299.14.

Madon, M., 1999. Basin types, Tectono-stratigraphic Provinces, and Structural Styles. The Petroleum Geology and Resources of Malaysia. PETRONAS, Kuala Lumpur, pp. 77–112.

Matheron, G., 1971. The Theory of Regionalized Variables and its Applications. Ecole des Mines, Fontainbleau, France 212 pp.

Morley, C.K., Back, S., Van Rensbergen, P., Crevello, P., Lambiase, J.J., 2003. Characteristics of repeated, detached, Miocene-Pliocene tectonic inversion events, in a large delta province on an active margin, Brunei Darussalam, Borneo. J. Struct. Geol. 25, 1147–1169. https://doi.org/10.1016/S0191-8141(02)00130-X.

Morley, C.K., Tingay, M., Hillis, R., King, R., 2008. Relationship between structural style, overpressures, and modern stress, Baram Delta Province, northwest Borneo. J. Geophys. Res.: Solid Earth 113, 1–23. https://doi.org/10.1029/2007JB005324.

Noorsalehi-Garakani, S., 2015. Fault Gouge in Sand-Clay Sequences - a First Look in 3D. PhD Thesis. pp. 1–222.

Parry, W.T., Chan, M.A., Nash, B.P., 2009. Diagenetic characteristics of the jurassic Navajo sandstone in the covenant oil field, central Utah thrust belt. AAPG Bull. 93, 1039–1061. https://doi.org/10.1306/04270908170.

Rawling, G.C., Goodwin, L.B., 2003. Cataclasis and particulate flow in faulted, poorly lithified sediments. J. Struct. Geol. 25, 317–331. https://doi.org/10.1016/S0191-8141(02)00041-X.

Rawling, G.C., Goodwin, L.B., Wilson, J.L., 2001. Internal architecture, permeability structure, and hydrologic significance of contrasting fault-zone types. Geology 29, 43–46. https://doi.org/10.1130/0091-7613(2001)029<0043:IAPSAH>2.0.CO;2.

Rawling, G.C., Goodwin, L.B., 2006. Structural record of the mechanical evolution of mixed zones in faulted poorly lithified sediments, Rio Grande rift, New Mexico, USA. J. Struct. Geol. 28, 1623–1639. https://doi.org/10.1016/j.jsg.2006.06.008.

Sandal, S.T., 1996. The Geology and Hydrocarbon Resources of Negara Brunei Darussalam. Brunei Museum Spec. Pub.,, Brunei Darussalam 243 pp. ISBN: 9991790004, 9789991790008.

Schmitz, B., Urai, J., Zee, W. Van Der, Holland, M., Littke, R., 2003. Transport properties and microstructural evolution in fault gouges - examples from a deltaic collapsed crest structure deformed at shallow depth. In: Proceedings, EAGE Conference on Fault and Top Seals.

Schultz, R.A., Fossen, H., 2008. Terminology for structural discontinuities. AAPG Bull. 92, 853–867. https://doi.org/10.1306/02200807065.

Shipton, Z.K., Evans, J.P., Kirchner, D., Kolesar, P.T., Williams, A.P., Heath, J., 2004. In: Baines, S.J., Worden, R.H. (Eds.), Analysis of CO2 Leakage through "low-permeability" Faults from Natural Reservoirs in the Colorado Plateau, Southern Utah, pp. 43–58.

Shipton, Z.K., Soden, A.M., Kirkpatrick, J.D., Bright, A.M., Lunn, R.J., 2006. How thick is a fault? Fault displacement-thickness scaling revisited. Earthquakes Radiated Energy Phys. Faulting 193–198.

Sibson, R.H., 2000. Fluid involvement in normal faulting. J. Geodyn. 29, 469–499. https://doi.org/10.1016/S0264-3707(99)00042-3.

Sigda, J.M., Goodwin, L.B., Mozley, P.S., Wilson, J.L., 1999. Permeability alteration in small-displacement faults in poorly lithified sediments: Rio Grande Rift, Central New Mexico. Geophys. Monogr. 113, 51–68. https://doi.org/10.1029/GM113.

Swanson, M.T., 1989. Sidewall ripouts in strike-slip faults. J. Struct. Geol. 11, 933–948.

Tan, D.N.K., Rahman, A.H.B.A., Anuar, A., Bait, B., Tho, C.K., 1999. West Baram Delta, the Petroleum Geology and Resources of Malaysia. Petroleum Nasional Berhad (PETRONAS), Kaula Lumpur, pp. 293–341.

Van der Zee, W., Urai, J.L., 2005. Processes of normal fault evolution in a siliciclastic sequence: a case study from Miri, Sarawak, Malaysia. J. Struct. Geol. 27, 2281–2300. https://doi.org/10.1016/j.jsg.2005.07.006.

Van der Zee, W., Urai, J.L., Richard, P.D., 2003. Lateral clay injection into normal faults. GeoArabia 8, 501–522.

Wannier, M., Lesslar, P., Lee, C., Raven, H., Sorkhabi, R., Ibrahim, A., 2011. Geological Excursions Around Miri, Sarawak. EcoMedia Software, Miri, pp. 279 10: 9834216033.

Watts, N.L., 1987. Theoretical aspects of cap-rock and fault seals for single- and two-phase hydrocarbon columns. Mar. Petrol. Geol. 4, 274–307. https://doi.org/10.1016/0264-8172(87)90008-0.

Woodcock, N.H., Miller, A.V.M., Woodhouse, C.D., 2014. Chaotic breccia zones on the Pembroke Peninsula, south Wales: evidence for collapse into voids along dilational faults. J. Struct. Geol. 69, 91–107. https://doi.org/10.1016/j.jsg.2014.09.019.

Woodcock, N.H., Mort, K., 2008. Classification of fault breccias and related fault rocks. Geol. Magn. 145, 435–440. https://doi.org/10.1017/S0016756808004883.

Woodcock, N.H., Omma, J.E., Dickson, J.A.D., 2006. Chaotic breccia along the Dent Fault, NW England: implosion or collapse of a fault void? J. Geol. Soc. 163, 431–446. https://doi.org/10.1144/0016-764905-067.